Reaction N(2 D) + CH 2 CCH 2 (Allene): An Experimental and Theoretical Investigation and Implications for the Photochemical Models of Titan

Gianmarco Vanuzzo, Luca Mancini, Giacomo Pannacci, Pengxiao Liang, Demian Marchione, Pedro Recio, Yuxin Tan, Marzio Rosi, Dimitrios Skouteris, Piergiorgio Casavecchia, et al.

ACS EARTH AND SPACE CHEMISTRY

http://pubs.acs.org/journal/aesccq

Article

Reaction N(^{2}D) + CH_2CCH_2 (Allene): An Experimental and Theoretical Investigation and Implications for the Photochemical Models of Titan

Gianmarco Vanuzzo, Luca Mancini, Giacomo Pannacci, Pengxiao Liang, Demian Marchione, Pedro Recio, Yuxin Tan,[§] Marzio Rosi, Dimitrios Skouteris, Piergiorgio Casavecchia, Nadia Balucani,* Kevin M. Hickson,* Jean-Christophe Loison, and Michel Dobrijevic

Cite This: https://doi.org/10.1021/acsearthspacechem.2c00183

Read Online

ACCESS | Metrics & More | Article Recommendations

ABSTRACT: We report on a combined experimental and theoretical investigation of the N(^{2}D) + CH_2CCH_2 (allene) reaction of relevance in the atmospheric chemistry of Titan. Experimentally, the reaction was investigated (i) under single-collision conditions by the crossed molecular beams (CMB) scattering method with mass spectrometric detection and time-of-flight analysis at the collision energy (E_c) of 33 kJ/mol to determine the primary products and the reaction micromechanism and (ii) in a continuous supersonic flow reactor to determine the rate constant as a function of temperature from 50 to 296 K. Theoretically, electronic structure calculations of the doublet C_3H_4N potential energy surface (PES) were performed to assist the interpretation of the experimental results and characterize the overall reaction mechanism. The reaction is found to proceed via barrierless addition of N(^{2}D) to one of the two equivalent carbon−carbon double bonds of CH_2CCH_2, followed by the formation of several cyclic and linear isomeric C_3H_4N intermediates that can undergo unimolecular decomposition to bimolecular products with elimination of H, CH_3, HCN, HNC, and CN. The kinetic experiments confirm the barrierless nature of the reaction through the measurement of rate constants close to the gas-kinetic rate at all temperatures. Statistical estimates of product branching fractions (BFs) on the theoretical PES were carried out under the conditions of the CMB experiments at room temperature and at temperatures (94 and 175 K) relevant for Titan. Up to 14 competing product channels were statistically predicted with the main ones at E_c = 33 kJ/mol being formation of *cyclic*-$CH_2C(N)CH$ + H (BF = 87.0%) followed by CHCCHNH + H (BF = 10.5%) and CH_2CCNH + H (BF = 1.4%) the other 11 possible channels being negligible (BFs ranging from 0 to 0.5%). BFs under the other conditions are essentially unchanged. Experimental dynamical information could only be obtained on the overall H-displacement channel, while other possible channels could not be confirmed within the sensitivity of the method. This is also in line with theoretical predictions as the other possible channels are predicted to be negligible, including the HCN/HNC + C_2H_3 (vinyl) channels (overall BF < 1%). The dynamics and product distributions are dramatically different with respect to those observed in the isomeric reaction N(^{2}D) + CH_3CCH (propyne), where at a similar E_c the main product channels are CH_2NH (methanimine) + C_2H (BF = 41%), c-C(N)CH + CH_3 (BF = 32%), and CH_2CHCN (vinyl cyanide) + H (BF = 12%). Rate coefficients (the recommended value is 1.7 (±0.2) × 10^{-10} cm^3 s^{-1} over the 50−300 K range) and BFs have been used in a photochemical model of Titan's atmosphere to simulate the effect of the title reaction on the species abundance (including any new products formed) as a function of the altitude.

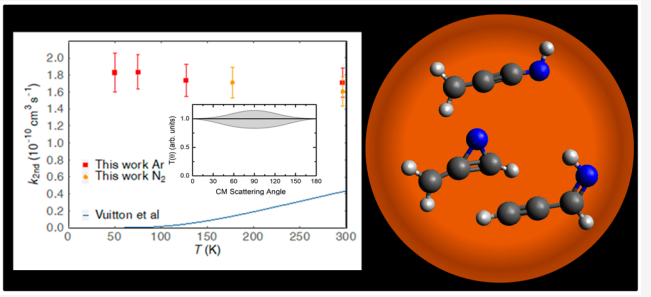

KEYWORDS: *atmospheric chemistry of Titan, prebiotic chemistry, reactivity of electronically excited species, nitrogen chemistry, formation of N-containing organic molecules*

1. INTRODUCTION

The study of other planets (or moons) of the solar system can be of great help in understanding prebiotic chemistry and the initial chemical evolution of Earth, where the presence of a biosphere and plate tectonics have drastically changed the primitive conditions that harbored life emergence.[1] In this respect, Titan (the massive moon of Saturn) has attracted a lot

Special Issue: Chemical Complexity in Planetary Systems

Received: June 15, 2022
Revised: September 8, 2022
Accepted: September 9, 2022

of attention[2] because its atmosphere is mainly composed of molecular nitrogen, like the terrestrial one, but sustains a very complex organic chemistry starting with methane, the second most abundant component (ca. 2% in the stratosphere and up to 5% close to the surface of the moon).[3] Among the organic species detected in trace amounts, the presence of nitriles and other N-containing organic species clearly indicates that active forms of nitrogen are at play.[4,5] In the upper atmosphere of Titan, chemistry is initiated by ionization and dissociation of the two main components (N_2 and CH_4), both induced by either VUV photons or collisions with energetic particles such as the electrons from the magnetosphere of Saturn.[4,5] These processes represent the starting point of a complex network of chemical reactions. Atomic nitrogen can be formed by N_2 EUV photodissociation or by dissociative electron impact as well as other processes like N_2^+ dissociative recombination. N atoms are produced not only in their ground ^4S state but also in their first electronically excited metastable states.[6] Among them, the $^2D_{3/2,5/2}$ state is of great relevance because its radiative lifetime is very long (the transition to the ground state is doubly forbidden) and is much more reactive than the ground ^4S state.[6] For this reason, N(^{2}D) reactions have been considered to play an important role since the first photochemical model of Titan developed by Yung et al. in 1984,[7] where N(^{2}D) reactions with methane[7] and acetylene[8] were included with estimated rate coefficients and products.

Because of the difficulty in producing N(^{2}D) in a controlled manner, until recently only fragmentary information was available from laboratory experiments on the reactions of N(^{2}D). After detailed investigation by means of the crossed molecular beam (CMB) method, supported by electronic structure calculations of the underlying potential energy surface (PES), now we know that N(^{2}D) has a complex chemical behavior, being able to insert into sigma bonds or to add to multiple bonds.[9−20] When reacting with hydrocarbons, molecular products possessing a novel C−N bond are formed.[9−14,18−20] Recent kinetic experiments performed with the CRESU technique at the relevant temperature for the conditions of the upper atmosphere of Titan have revealed that the rate constants for several important N(^{2}D) reactions are considerably larger[21,22] or smaller[23] than those determined by previous experiments above 200 K.[24−26] The inclusion of these data in updated versions of a photochemical model of the atmosphere of Titan have demonstrated the importance of this approach in making the model more accurate.[21−23]

Methylacetylene (propyne) and allene (propadiene) are two structural isomers of gross formula C_3H_4 that are formed in the upper atmosphere of Titan. Both are predicted to be present by all photochemical models in similar amounts because their main formation mechanism is considered to be the reaction H + C_3H_5, producing both isomers with the same yield. However, while methylacetylene was first detected during the Voyager mission,[27−29] attempts to detect allene were unsuccessful[30−32] until the recent unambiguous detection by Lombardo et al.[33] by means of a Texas Echelle Cross Echelle Spectrograph (TEXES) mounted on the NASA Infrared Telescope Facility. Allene has an abundance of 6.9 ($\pm$0.8) $\times$ 10^{-10} at an altitude of 175 km and is less abundant than methylacetylene by a factor of 8.2 ($\pm$1.1) at 150 km if a vertically increasing profile is assumed.[33]

The reactions between atomic nitrogen in its ^{2}D state and both methylacetylene and allene have already been included in photochemical models with estimated rate coefficients and product branching fractions (BFs).[4,5] In the case of the N(^{2}D) + CH_2CCH_2 reaction, by analogy with similar systems, Loison et al.[4] suggested that the main reaction channel is that leading to vinyl cyanide (cyanoethylene) + H with a global rate coefficient of $2.3 \times 10^{-10} \times \exp(-503/T)$. However, according to the present B3LYP/CCSD(T) calculations, there are many additional open reactive channels correlating with the reactants

$$N(^2D) + CH_2CCH_2 \rightarrow CH_2CHCN + H \quad \Delta H_0^\circ = -444\ \text{kJ/mol} \tag{1a}$$

$$N(^2D) + CH_2CCH_2 \rightarrow C_2H_3 + HCN \quad \Delta H_0^\circ = -434\ \text{kJ/mol} \tag{1b}$$

$$N(^2D) + CH_2CCH_2 \rightarrow C_2H_4 + CN \quad \Delta H_0^\circ = -381\ \text{kJ/mol} \tag{1c}$$

$$N(^2D) + CH_2CCH_2 \rightarrow C_2H_3 + HCN \quad \Delta H_0^\circ = -368\ \text{kJ/mol} \tag{1d}$$

$$N(^2D) + CH_2CCH_2 \rightarrow CHCCHNH + H \quad \Delta H_0^\circ = -300\ \text{kJ/mol} \tag{1e}$$

$$N(^2D) + CH_2CCH_2 \rightarrow CH_2CCNH + H \quad \Delta H_0^\circ = -271\ \text{kJ/mol} \tag{1f}$$

$$N(^2D) + CH_2CCH_2 \rightarrow c\text{-}H_2CC(N)CH + H \quad \Delta H_0^\circ = -226\ \text{kJ/mol} \tag{1g}$$

$$N(^2D) + CH_2CCH_2 \rightarrow CH_2CCH + NH \quad \Delta H_0^\circ = -175\ \text{kJ/mol} \tag{1h}$$

$$N(^2D) + CH_2CCH_2 \rightarrow CH_3CCN + H \quad \Delta H_0^\circ = -148\ \text{kJ/mol} \tag{1i}$$

$$N(^2D) + CH_2CCH_2 \rightarrow c\text{-}H_2CC(NH)C + H \quad \Delta H_0^\circ = -96\ \text{kJ/mol} \tag{1j}$$

$$N(^2D) + CH_2CCH_2 \rightarrow CHCH_2CN + H \quad \Delta H_0^\circ = -96\ \text{kJ/mol} \tag{1k}$$

$$N(^2D) + CH_2CCH_2 \rightarrow CHCHCNH + H \quad \Delta H_0^\circ = -90\ \text{kJ/mol} \tag{1l}$$

$$N(^2D) + CH_2CCH_2 \rightarrow CH_3 + CCNH \quad \Delta H_0^\circ = -72\ \text{kJ/mol} \tag{1m}$$

$$N(^2D) + CH_2CCH_2 \rightarrow CH_3CC + NH \quad \Delta H_0^\circ = -4\ \text{kJ/mol} \tag{1n}$$

where the enthalpies of reactions reported are those calculated in the present work at the CCSD(T) level (see section 3.1). There are eight H-displacement channels leading to eight different C_3H_3N isomeric species, two NH formation channels,

https://doi.org/10.1021/acsearthspacechem.2c00183
ACS Earth Space Chem. XXXX, XXX, XXX−XXX

and four C−C bond-breaking channels leading to HCN, HNC, CN, and CH_3 formation.

In addition, an H_2-elimination channel is also possible through a roaming mechanism (see section 5.1)

$$N(^2D) + CH_2CCH_2 \rightarrow CH_2CCN + H_2 \quad \Delta H_0^\circ = -404\ \text{kJ/mol} \qquad (1o)$$

with the enthalpy of reaction obtained at the same level of calculations as the other channels.

In this manuscript, we report on a combined experimental and theoretical investigation of the reaction $N(^2D)$ + CH_2CCH_2. More specifically, we employed the CMB technique to explore the nature of the primary products and their BFs and the CRESU technique to measure the global rate coefficient at temperatures of interest for Titan. In addition, we performed dedicated electronic structure calculations of the underlying PES and RRKM (Rice−Ramsperger−Kassel−Marcus) estimates of the product BFs. The information so obtained are used in a photochemical model of Titan's atmosphere to simulate the effect of this reaction on the species abundance (including any new products formed) as a function of altitude. A comparison with the reaction mechanism of the reaction involving the methylacetylene isomer will also be presented to highlight similarities and differences.

2. EXPERIMENTAL SECTION

2.1. Crossed Molecular Beam Experiments. The scattering experiments were carried out using an improved version of the CMB apparatus described previously.[34−37] Briefly, two supersonic beams of the reactants are crossed at a specific angle (90°) in a large scattering chamber kept in the low 10^{-6} mbar range in operating conditions to ensure single-collision conditions. The species of each beam are characterized by a well-defined velocity and direction and are made to collide only with the atoms/molecules of the other beam, allowing us to observe the consequences of well-defined reactive molecular collisions. The detection system consists of a tunable electron impact ionizer, a quadrupole mass filter, and a Daly detector. The ionizer is located in the innermost region of a triply differentially pumped ultrahigh-vacuum chamber, which is maintained in the 10^{-11} mbar pressure range in operating conditions by extensive turbo- and cryopumping. The whole detector unit can be rotated in the collision plane around an axis passing through the collision center, and the velocities of both reactants and products are derived from single-shot and pseudorandom, respectively, time-of-flight (TOF) measurements.

A supersonic beam of N atoms was produced by means of a radio frequency (rf) discharge beam source described in refs 38 and 39. We operated by discharging 250 W of rf power on a dilute (2.5%) mixture of N_2 in He (stagnation pressure of 125 mbar), expanded through a 0.48 mm diameter quartz nozzle followed by a boron nitride skimmer (diameter of 0.8 mm) placed at a distance of about 6 mm from the front of the nozzle. The peak velocity and speed ratio were 2354 m/s and 5.9, respectively. A high dissociation of molecular nitrogen (about 60%) is achieved. Nitrogen atoms are produced in a distribution of electronic states as shown in a previous characterization by means of Stern−Gerlach magnetic analysis.[39] Seventy-two percent of the N atoms were found to be produced in the ground ^4S state, while 21% and 7% are produced in the ^2D and ^2P excited state, respectively. Under the present experimental conditions, the use of a beam also containing nitrogen atoms in the electronic ^4S and ^2P states is not a problem since the rate coefficients for reactions between $N(^4S)$ and unsaturated hydrocarbons are extremely small, while $N(^2P)$ is known to mostly undergo physical quenching.[6] We expect a similar situation also in the case of the title reaction. Indeed, according to the present theoretical characterization of the title reaction, the reactivity of the $N(^4S)$ state is not expected to be significant as we could not locate any addition intermediate in low-energy quartet states, while the H-abstraction channel is endothermic by 55 kJ/mol at the present level of calculations (and, therefore, it is not accessible under the conditions of our experiments or under the condition of the atmosphere of Titan).

A supersonic beam of allene was generated by expanding 400 mbar of neat allene through a 100 μm diameter stainless-steel nozzle kept at room temperature. A collimating stainless-steel skimmer of 0.8 mm diameter was placed 7 mm from the front of the nozzle. The peak velocity and speed ratio were 696 m/s and 4.5, respectively.

The angular divergence, which is defined by the collimating slits placed after the skimmers, is 2.4° for the N beam and 3.8° for the allene beam. The detector has a nominal angular resolution for a point collision zone of 1.1°.

The resulting collision energy is 33 kJ/mol, while the angle of the center-of-mass (CM) velocity vector in the laboratory (LAB) reference frame with respect to the velocity vector associated with the atomic nitrogen beam is $\Theta_{CM} = 40.7°$. The product angular distribution, $N(\Theta)$, was recorded by means of a tuning-fork chopper (for background subtraction) mounted between the nozzle and the skimmer defining the allene beam (modulation frequency of 160 Hz). The velocity distributions of the products were measured by the pseudorandom chopping technique using four 127-bit open-closed sequences based on the cross-correlation method. High time resolution was obtained by spinning the TOF disk, located before the entrance slit of the detector, at 328 Hz, corresponding to a dwell time of 6 μs/ch. The flight length was 24.3 cm.

The measurements have been carried out in the LAB reference frame. However, in order to obtain quantitative information on the scattering process, it was necessary to move from the LAB to the CM frame; in this way, it is possible to derive the CM product flux distribution $I_{CM}(\theta, E'_T)$, i.e., the double-differential cross section. This can be factorized into two independent functions: a function depending only on the scattering angle, $T(\theta)$, and a function depending on the velocity, $P(u)$, or translational energy, $P(E'_T)$, of the products.[35,36] It is important to notice that because of the finite resolution of the experimental conditions, such as the angular and velocity spread of the reactant beams and the angular resolution of the detector, the conversion from the LAB to the CM reference system is not single valued. Therefore, the analysis of the LAB data have been performed by *forward convoluting* tentative CM distributions over the experimental conditions. In other words, the CM angular, $T(\theta)$, and translation energy, $P(E'_T)$, distributions are assumed, averaged, and transformed into the LAB frame for comparison with the experimental distributions. The procedure is repeated until a satisfactory fit of the experimental data is achieved.[34]

2.2. Kinetics Experiments. All of the kinetic measurements reported here were conducted using a continuous

https://doi.org/10.1021/acsearthspacechem.2c00183
ACS Earth Space Chem. XXXX, XXX, XXX−XXX

supersonic flow (Laval nozzle) reactor, whose main features have been described in detail previously.[40,41] The original apparatus has been modified over the years to allow both ground state and excited state atomic radicals such as $C(^3P)$,[42,43] $H(^2S)$,[44,45] $O(^1D)$,[46,47] and recently, $N(^2D)$[21−23,48] to be detected in the vacuum ultraviolet (VUV) wavelength range. To perform kinetic measurements over a range of low temperatures, three different Laval nozzles were utilized during this investigation, allowing four different temperatures (50, 75, 127, and 177 K) to be accessed (one nozzle was used with two carrier gases), in addition to room temperature (296 K) in the absence of a nozzle and at a significantly reduced flow velocity. As previous measurements of $N(^2D)$ quenching have shown that relaxation is slow with both Ar[49] and N_2,[50] it was possible to use both of these as carrier gases. The flow characteristics of the nozzles used during this study are listed in Table 1 of Nuñez-Reyes et al.[21] $N(^2D)$ atoms were produced indirectly during this study as a product of reaction 2a

$$C(^3P) + NO \rightarrow N(^2D, {}^4S) + CO \quad (2a)$$

$$\rightarrow O(^3P) + CN \quad (2b)$$

in common with previous work[21−23,48] due to the lack of precursor molecules to produce this species photolytically in an appropriate wavelength range. The yield of total atomic nitrogen ($N(^2D)$ + $N(^4S)$) has been estimated to be approximately three times greater than the yield of ground state atomic oxygen at room temperature.[51] Ground state atomic carbon, $C(^3P)$, was produced in situ by the pulsed laser photolysis of carbon tetrabromide (CBr_4) at 266 nm. CBr_4 was introduced into the flow by passing a small flow of the carrier gas over solid CBr_4 held in a separate container at a known pressure and room temperature. CBr_4 concentrations were estimated to be lower than 4×10^{13} cm^{-3} based on its saturated vapor pressure, while NO concentrations were in the range $3.0-6.4 \times 10^{14}$ cm^{-3}.

In addition to $C(^3P)$, $C(^1D)$ atoms were also generated during CBr_4 photodissociation with a $C(^1D)/C(^3P)$ ratio measured in earlier work of 0.1−0.15.[42] C(1D) atoms are expected to react rapidly with NO[52] to form similar products to the ground state reaction (reactions 2a and 2b) and/or be quenched rapidly to the ground state when N_2 is used as the carrier gas.[53] The photolysis laser beam diameter was reduced from 12 to 5 mm using an afocal telescope, allowing significantly higher pulse energies (30−40 mJ) to be used than in previous kinetic studies (20−25 mJ). As larger $C(^3P)$ (and $N(^2D)$) concentrations were generated, a significant improvement in the signal-to-noise ratio was observed.

$N(^2D)$ atoms were detected directly during this study by pulsed laser-induced fluorescence at 116.745 nm through the $2s^22p^3\ ^2D^\circ-2s^22p^2(^3P)3d\ ^2F$ electronic transition. The procedure used to generate tunable coherent radiation around this wavelength by third-harmonic generation of a monochromatic UV source focused into a cell containing rare gas has been described in detail in previous work.[48] Upon exiting the cell, the VUV probe beam was collimated by a MgF_2 lens and directed into the reactor through a 75 cm long side arm containing a series of circular diaphragms to trap the divergent UV beam. The side arm itself was attached to the reactor at the level of the observation axis, so that the VUV beam crossed the cold supersonic flow at right angles. In this way, it was also perpendicular to the detector. This arrangement ensured that only a tiny fraction of the residual UV light reached the detector. Fluorescence emission from excited $N(^2D)$ atoms in the flow, on resonance with the probe laser, was detected by a solar blind photomultiplier tube (PMT) which was protected from reactive gases in the chamber by a LiF window. A LiF lens placed between the window and the PMT focused the emitted light onto the PMT photocathode. As atmospheric O_2 possesses numerous absorption features in this region of the electromagnetic spectrum, the zone between the LiF window and the PMT was maintained under vacuum. In contrast to previous work, the output of the PMT was fed directly into a boxcar integrator without the need for prior amplification. Nevertheless, the first 5 μs following the photolysis laser pulse remained unexploitable (compared to 15 μs in previous work when an amplifier was used) due to scattering of the photolysis laser beam by the precursor CBr_4 molecules in the supersonic flow. Typically, between 70 and 100 time points (including approximately 15 time points to establish the baseline) were recorded for each kinetic profile with 30 laser shots averaged at each time point. All gas flows (Messer Ar 99.999%, N_2 99.995%, Linde Xe 99.999%, Sigma-Aldrich CH_2CCH_2 >95%, Air Liquide NO 99.9%) were controlled by calibrated mass flow controllers, allowing the coreagent NO and CH_2CCH_2 concentrations to be determined accurately.

3. COMPUTATIONAL DETAILS

3.1. Electronic Structure Calculations. The $N(^2D)$ + CH_2CCH_2 reaction has been analyzed by considering the lowest doublet electronic state of the C_3H_4N system. The potential energy surface has been characterized through optimization of the most stable stationary points at the B3LYP[54,55] level of theory in conjunction with the correlation-consistent valence-polarized set aug-cc-pVTZ.[56−58] Harmonic vibrational frequencies have been computed at the same level of theory in order to check the nature of the stationary points, i.e., minimum if all frequencies are real, saddle point if there is one and only one imaginary frequency. Intrinsic reaction coordinate (IRC) calculations have been performed to assign the nature of each saddle point.[59,60] More accurate values of energy of all of the stationary points have been calculated at the higher level of calculation CCSD(T)[61−63] with the same basis set aug-cc-pVT. The zero-point energy (ZPE) correction, computed using the scaled harmonic vibrational frequencies evaluated at the B3LYP/aug-cc-pVTZ level, has been added to both the B3LYP and the CCSD(T) energies to correct them at 0 K. The energy of $N(^2D)$ has been evaluated by adding the experimental[64] separation $N(^4S)-N(^2D)$ of 230.0 kJ/mol to the energy of $N(^4S)$ at all levels of calculation. All calculations have been performed using Gaussian 09,[65] while the analysis of the vibrational frequencies has been carried out using AVOGADRO.[66,67]

3.2. RRKM Calculations. RRKM calculations for the $N(^2D)$ + CH_2CCH_2 reaction have been performed using a code developed in our group for this purpose.[11−13] As suggested by the RRKM scheme,[68] the microcanonical rate constant, $k(E)$, for a specific reaction at a specific total energy is given by the expression

$$k(E) = \frac{N_{TS}(E)}{h\rho_T(E)}$$

where $N_{TS}(E)$ is the sum of states of the transition state at energy E, $\rho_T(E)$ is the reactant density of states at energy E, and h is Planck's constant. The partition function has been

https://doi.org/10.1021/acsearthspacechem.2c00183
ACS Earth Space Chem. XXXX, XXX, XXX−XXX

used to perform an inverse Laplace transform in order to evaluate the rotational densities of states both for the reactants and for the transition states. Subsequently, the rotational densities of states were convoluted with the corresponding vibrational ones using a direct count algorithm. Finally, the sum of states has been obtained by integrating the density of states with respect to the energy. Where possible, tunneling (as well as quantum reflection) has been considered by using the corresponding imaginary frequency of the transition state and calculating the tunneling probability for the corresponding Eckart barrier. For barrierless dissociation channels, the variational RRKM approach is normally used.[69] In this case, however, that approach could not be employed because of some difficulties in the electronic structure calculations of the intermediate points. Considering that the channels of interest are characterized by energetically monotonic exit paths, the transition state has been assumed as the products at infinite separation. The way we avoid problems arising from the different number of degrees of freedom between the reactants and the transition state is by not including the 2D part of the overall rotation in the RRKM treatment of the reactants (leaving only the "prolate" 1D contribution).

After the calculation of all microcanonical rate constants, a Markov (stochastic) matrix was set up for all intermediates and final channels to derive the product branching fractions for the overall reaction. $k(E)$ is subsequently Boltzmann averaged for each temperature of interest to yield $k(T)$.

4. EXPERIMENTAL RESULTS

4.1. CMB Experiments. Preliminary measurements were made at different mass-to-charge ratios (m/z). The signal was observed at the following: (1) m/z = 53 ($C_3H_3N^+$), which corresponds to the parent ion of molecular products in the H-displacement channels; (2) m/z = 52 ($C_3H_2N^+$), which corresponds either to the parent ion of the molecular product associated with the H_2-elimination channel or the −1 daughter ion associated with the H-displacement channels; (3) m/z = 51 (C_3HN^+) and 50 (C_3N^+), which correspond to the daughter ions of cases 1 and 2. In this range of masses, the signal at m/z = 51 was found to be the most intense one with the highest signal-to-noise (S/N) ratio (with a 50 s counting time, the S/N ratios were 46, 54, 82, and 30, respectively). During data analysis, no features of the measured distributions pointed to the presence of an H_2-elimination channel, so the signal recorded at m/z between 50 and 53 can be attributed to the H-displacement channels 1a, 1e−1g, and 1i−1l. No signal was detected at m/z = 27, which rules out (within our sensitivity, i.e., BR ≤ 5%) channels 1b and 1d, leading to HCN and HNC formation, respectively.

We also attempted to measure reactive scattering distributions at m/z = 26 and 28 to characterize channel 1c leading to CN + C_2H_4. Unfortunately, we have not been able to verify if a small reactive scattering signal is present at those masses because of (a) a strong interfering signal at m/z = 28 associated with the elastic scattering of undissociated molecular nitrogen from the primary beam and (b) an interfering signal at m/z = 26 also coming from the primary beam. This is probably caused by the presence in the gas line of traces of CO_2 which dissociates and reacts with N/N_2 forming CN in the plasma produced by the radio frequency discharge.

Finally, since a CH_3-loss channel is possibly open (channel 1m) and considering that the cofragment distributions at m/z = 39 (C_2NH^+) could not be measured because of an intense elastic signal associated with the dissociative ionization of allene, we tried to record a TOF distribution at m/z = 15 (CH_3^+) by using the soft-ionization approach (17 eV and an emission current of 1.50 mA). After an accumulation time of 45 min, no signal was observed at Θ = 40°. This ruled out, within our sensitivity, the occurrence of channel 1m.

The full set of final data, that is the LAB angular distributions and TOF spectra at Θ = 24°, 32°, 40°, and 48° (counting times ranging from 2 to 3 h per angle depending on the signal intensity), were recorded at m/z = 51.

To better illustrate the CMB experimental results and discuss the dynamics of the various reaction channels, it is useful to observe the velocity vector (so-called Newton) diagram shown in Figure 1 (bottom), which describes the kinematics of the experiment. The circles are drawn assuming that all of the available energy is converted into product translational energy, and therefore, they delimit the maximum speed that the various indicated products can assume in the CM frame. Only the products associated with the most exothermic H-displacement channels 1a, 1e, 1f, and 1g are shown because we expect a negligible contribution from the other isomers (see Discussion).

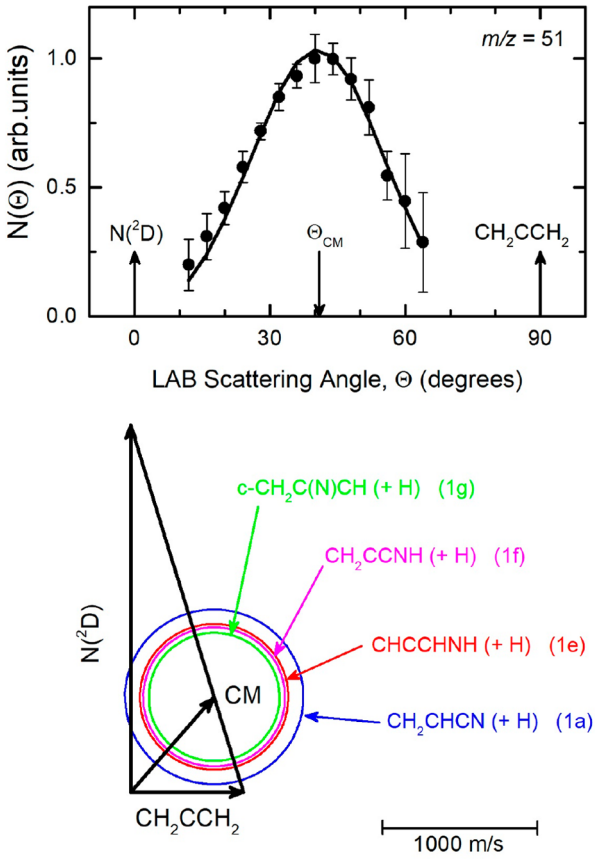

Figure 1. (Top) LAB angular distribution at m/z = 51 for the N(^{2}D) + allene reaction at E_c = 33 kJ/mol. The solid line represents the calculated distribution when using the best-fit CM functions of Figure 3. (Bottom) Velocity vector (Newton) diagram of the CMB experiment. The radius of each circle represents the maximum speed that the indicated product can attain in the center-of-mass reference frame if all available energy is channeled into product recoil energy.

https://doi.org/10.1021/acsearthspacechem.2c00183
ACS Earth Space Chem. XXXX, XXX, XXX−XXX

The LAB angular distribution recorded at $m/z = 51$ is shown in Figure 1 (top). It is characterized by a bell shape and peaks at Θ_{CM}. The relatively small extension confirms that the products are kinematically constrained in small Newton circles around the CM angle, in line with those shown in Figure 1 (bottom). The product TOF spectra at four selected LAB angles are displayed in Figure 2. As can be seen, the TOF spectra are characterized by a single peak, centered around 250 μs.

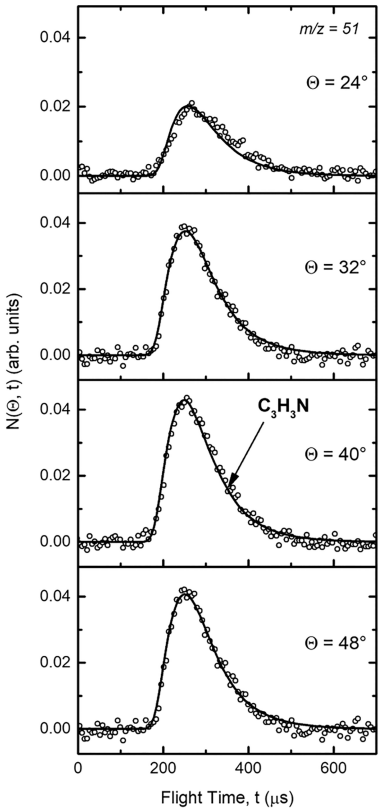

Figure 2. Time-of-flight distributions for $m/z = 51$ at angles $\Theta = 24°$, 32°, 40°, and 48°. Open circles: experimental data. Solid lines: calculated distributions when using the best-fit CM functions of Figure 3.

The best-fit CM functions are shown in Figure 3. As can be seen, the best-fit CM angular distribution is isotropic. In addition, the functions that allow an acceptable fit of the data (delimited by the shaded areas in Figure 3, top) are all backward−forward symmetric, indicating that the title reaction proceeds through the formation of a long-lived complex.[70] We recall that in this case, the collision complex survives several rotational periods, losing memory of the initial approach directions of the reactants. At the same time, its lifetime is long enough to allow the energy available to the system to be statistically distributed among the various degrees of freedom. This is an important indication as it sustains the applicability of an RRKM approach to derive the product branching fractions.

The shape of the $P(E'_T)$ reveals the extent of energy release, which give us a criterion, according to the energy conservation rule,[70] to establish which products of general formula C_3H_3N are compatible with the experimental distributions. In our experimental conditions, the translational energy distribution has a maximum at about 60 kJ/mol and extends up to about

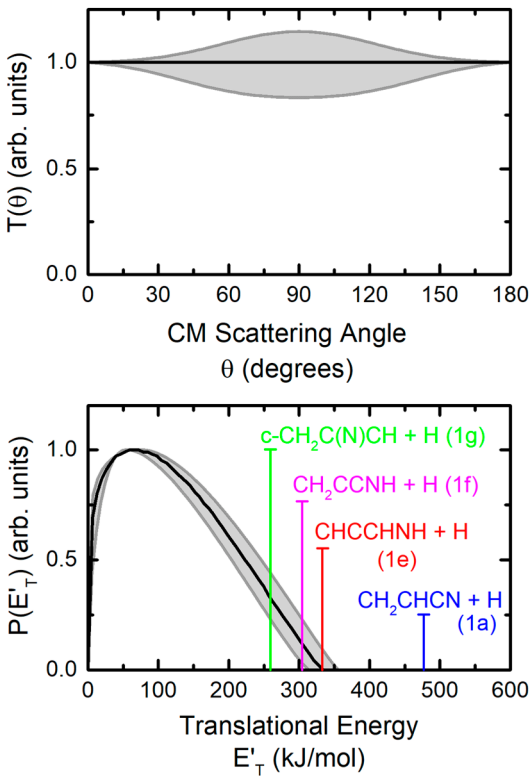

Figure 3. Best-fit angular (top) and translational energy (bottom) distributions, $T(\theta)$ and $P(E'_T)$, in the center of mass reference system for the $N(^2D)$ + allene reaction. Shaded areas represent the error bars. Arrows in the graph of $P(E'_T)$ indicate the total energy $(E_c - \Delta H^0_0)$ associated with the formation of the four indicated isomers with formula C_3H_3N.

335(±20) kJ/mol. The average product translational energy, defined as $\langle E'_T \rangle = \sum P(E'_T)E'_T / \sum P(E'_T)$, is about 116 kJ/mol and corresponds to an average fraction, $\langle f'_T \rangle$, of 0.35 of the total available energy ($E_{tot} = E_c - \Delta H^\circ_0$) for the most exothermic H-displacement channel that was found to contribute significantly to the overall yield, namely, channel 1e (CHCCHNH + H) (see section 5.2). Given the similar enthalpy changes associated with the most exothermic H-displacement channels 1a, 1e, 1f, and 1g and the expected similar reaction mechanisms, we have not been able to disentangle the contributions of each channel to the recorded signal. We must rely on electronic structure and RRKM calculations to derive the product branching fractions (see sections 5.1 and 5.2).

4.2. Kinetic Results. The analysis of the kinetic data was simplified by employing the pseudo-first-order approximation by using large excess concentrations of the coreagents [NO] and [CH_2CCH_2] with respect to the minor reagents $C(^3P)$ and $N(^2D)$. Under these conditions, the $N(^2D)$ fluorescence signal should follow a temporal profile with a biexponential form given by

$$I_{N(^2D)} = A(\exp(-k'_a t) - \exp(-k'_b t)) \quad (3)$$

where A is the theoretical maximum signal amplitude when the first term in expression 3 is equal to zero, k'_a is the pseudo-first-order rate constant for $N(^2D)$ loss, k'_b is the pseudo-first-order rate constant for $N(^2D)$ formation, and t is time. Although more early time points were exploitable in this work than in

https://doi.org/10.1021/acsearthspacechem.2c00183
ACS Earth Space Chem. XXXX, XXX, XXX−XXX

previous studies of N(^{2}D) reactions as explained above, an analysis employing a single-exponential function

$$I_{N(^2D)} = A \exp(-k_a' t) \quad (4)$$

was still employed due to the difficulty of performing accurate fits during the rising part of the temporal profiles. The fitting procedure was applied only to those data points obeying a single-exponential decay law, essentially excluding data within the first 10−20 μs following the photolysis laser pulse. Some typical decay traces recorded at 127 K are shown in Figure 4.

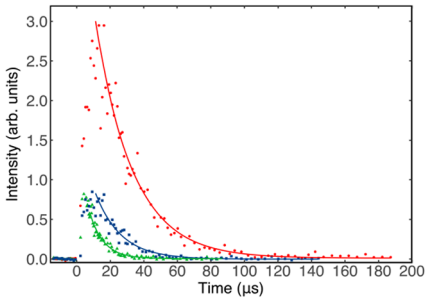

Figure 4. N(^{2}D) fluorescence emission intensity as a function of time between photolysis and probe lasers, recorded at 127 K: (solid red circles) without CH_2CCH_2; (solid blue squares) [CH_2CCH_2] = 1.1 × 10^{14} cm^{-3}; (solid green triangles) [CH_2CCH_2] = 4.3 × 10^{14} cm^{-3}. [NO] = 4.7 × 10^{14} cm^{-3} for all traces. Solid lines represent nonlinear Levenberg−Marquardt fits to the data using expression 4.

In common with earlier work, it is important to consider the potential effects of secondary chemistry on the kinetics of the N(^{2}D) + CH_2CCH_2 reaction. As the C(^{3}P) + CH_2CCH_2 reaction is rapid at low temperature,[71] leading to various C_4H_4 isomers and H atoms as the primary products,[72,73] it competes with reactions 2a and 2b, lowering the production of N(^{2}D) atoms in the flow. This can be seen clearly in Figure 4, where the peak N(^{2}D) fluorescence signal of the experiments performed in the presence of CH_2CCH_2 (green triangles and blue squares) is significantly reduced compared to the experiment where CH_2CCH_2 is absent (red circles). A detailed analysis of the secondary reactions that could arise in such studies of the reactions of N(^{2}D) atoms with unsaturated hydrocarbons has already been presented in previous work.[21,22] In the present case, secondary reactions such as those between the CN product of reaction 2b in particular and CH_2CCH_2 lead to the formation of various unsaturated hydrocarbons containing a cyano group (such as cyanoallene)[74] and H atoms, neither of which are expected to produce N(^{2}D) atoms through subsequent reactions. Similarly, the reaction between the various C_4H_4 isomers that could be present in the flow and NO coreagent are not expected to lead to N(^{2}D) production either, although no information on these processes could be found in the literature. Overall, considering the various secondary reactions that could be occurring in the flow, it seems unlikely that these processes would have an important influence on the accuracy of the present kinetic measurements.

Temporal profiles such as those shown in Figure 4 were recorded at a minimum of five different CH_2CCH_2 concentrations at each temperature. The values of the pseudo-first-order rate constants k_a', derived from fits to the data using eq 4, were then plotted as a function of the CH_2CCH_2 concentration to yield second-order plots such as those shown in Figure 5. Weighted fits to these data yielded the second-order rate constant from the slope.

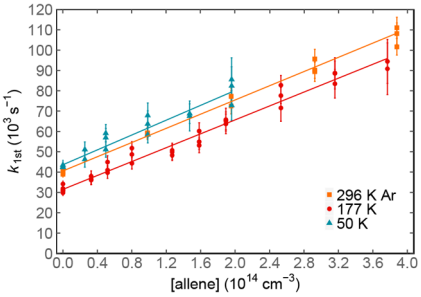

Figure 5. Measured pseudo-first-order rate constant as a function of [CH_2CCH_2]: (orange solid squares) data recorded at 296 K; (red solid circles) data recorded at 177 K; (blue solid triangles) data recorded at 50 K. Solid lines represent the weighted linear least-squares fits to the data. Errors on individual data points are shown at the level of a single standard deviation and are derived from the nonlinear fits of traces similar to those displayed in Figure 4.

The large y-axis intercept values of these plots (Figure 5) arise mostly from the reaction between N(^{2}D) and NO, where NO is constant for any series of measurements at a given temperature. For example, at 177 K, considering [NO] = 4.1 × 10^{14} cm^{-3} and $k_{N(^2D)+NO}$(177 K) = 8 × 10^{-11} cm^3 s^{-1},[48] we obtain 32 800 s^{-1}, a value that is seen to correspond well to the measured intercept in Figure 5. When a similar calculation is performed at 50 K however ([NO] = 4.2 × 10^{14} cm^{-3} and $k_{N(^2D)+NO}$(50 K) = 13 × 10^{-11} cm^3 s^{-1}),[48] we obtain 54 600 s^{-1}, somewhat larger than the measured intercept value here of 43 600 s^{-1}. This discrepancy was also observed in our other recent studies of N(^{2}D) reactions (N(^{2}D) + C_2H_2[21] and N(^{2}D) + C_2H_4[22]), suggesting that the rate constant for $k_{N(^2D)+NO}$(50 K) might be slightly overestimated in the preliminary study of Nunez-Reyes et al.[48]

The measured second-order rate constants are plotted as a function of temperature in Figure 6, while these values are summarized in Table 1 alongside other relevant experimental parameters.

5. THEORETICAL RESULTS

5.1. Potential Energy Surface. The potential energy surface is shown in Figure 7. Seven minima have been

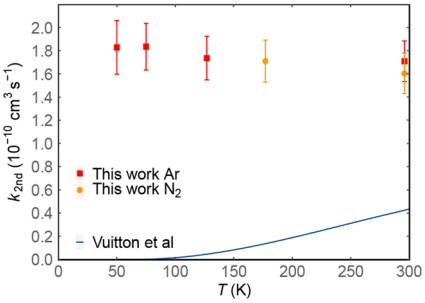

Figure 6. Second-order rate constants for the N(^{2}D) + allene reaction as a function of temperature: (solid red squares) this work Ar carrier gas; (solid orange circles) this work N_2 carrier gas. Solid dark blue line represents the current recommendation for the rate constants of the N(^{2}D) + allene reaction used in the models of Vuitton et al.[5] and Krasnopolsky.[75]

https://doi.org/10.1021/acsearthspacechem.2c00183
ACS Earth Space Chem. XXXX, XXX, XXX−XXX

Table 1. Measured Second-Order Rate Constants for the $N(^2D) + CH_2CCH_2$ Reaction

T/K	N[b]	$[CH_2CCH_2]/10^{14}$ cm^{-3}	$[NO]/10^{14}$ cm^{-3}	$k_{N(^2D)+CH_2CCH_2}/10^{-11}$ cm^3 s^{-1}
296 (N_2)	22	0−4.9	6.4	(16.0 ± 1.7)[c]
296 (Ar)	18	0−4.8	6.3	(17.1 ± 1.8)
177 ± 2[a]	32	0−3.8	4.1	(17.1 ± 1.8)
127 ± 2	30	0−4.3	4.7	(17.4 ± 1.9)
75 ± 2	15	0−2.1	3.0	(18.3 ± 2.0)
50 ± 1	16	0−2.0	4.2	(18.3 ± 2.3)

[a]Uncertainties on the calculated temperatures represent the statistical (1σ) errors obtained from Pitot tube measurements of the impact pressure. [b]Number of individual measurements. [c]Uncertainties on the measured rate constants represent the combined statistical (1σ) and estimated systematic (10%) errors.

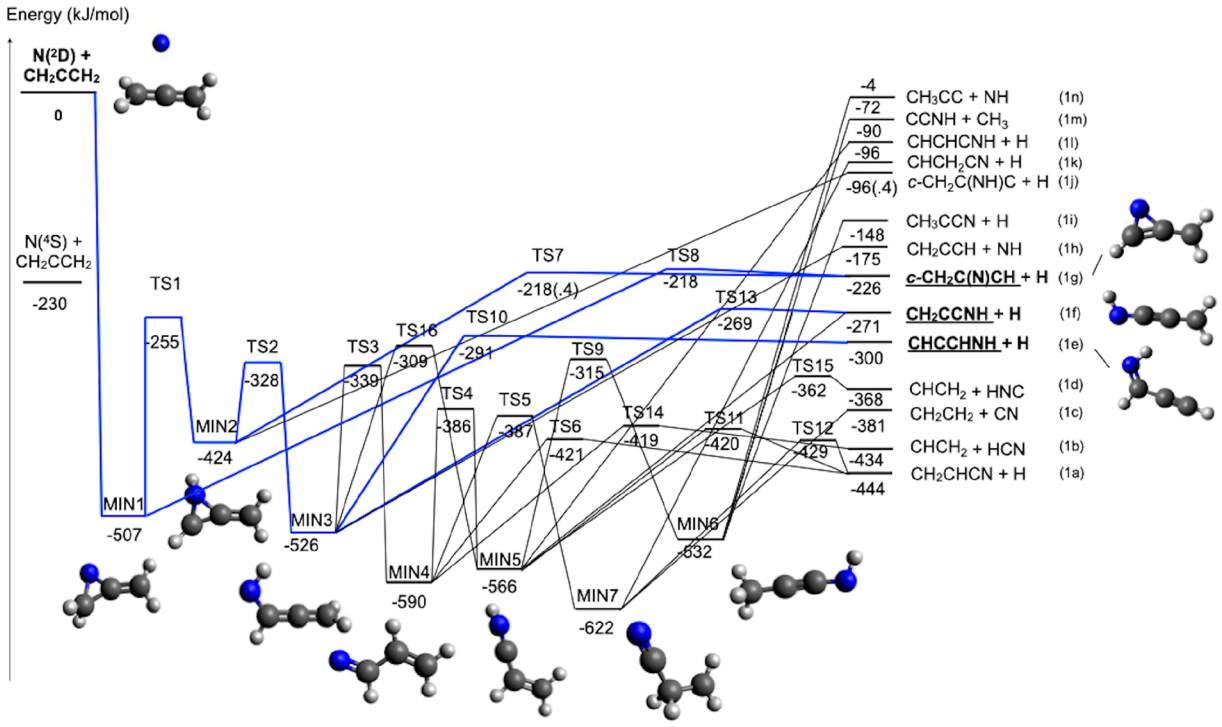

Figure 7. Schematic representation of the potential energy surface for the reaction $N(^2D) + CH_2CCH_2$ with energies evaluated at the CCSD(T)/aug-cc-pVTZ level of theory (see text). Structures of the heavier coproducts from the three main product channels are shown as well as the structures of all intermediates. Blue lines indicate the main pathways leading to the underlined three (statistically predicted) main products.

identified (MIN1−7) linked by seven transition states (TS1, connecting MIN1 and MIN2; TS2, connecting MIN2 and MIN3; TS3, connecting MIN3 and MIN4; TS4, connecting MIN4 and MIN5; TS5, connecting MIN4 and MIN7; TS9, connecting MIN5 and MIN6; TS16, connecting MIN3 and MIN5). As expected, the initial step is represented by the barrierless attack of the nitrogen atom to one of the two double bonds of allene, leading to the formation of the cyclic intermediate MIN1, located at −507 kJ/mol (at the CCSD(T) level) with respect to the reactant asymptote. This first intermediate can directly dissociate to products via fission of a C−H bond, leading to c-$CH_2C(N)CH$ + H (channel 1g). An exit barrier of +8 kJ/mol with respect to the products asymptote (TS8) is present. Alternatively, MIN1 can isomerize to MIN2 (by overcoming TS1). MIN2 can also dissociate into the products associated with channel 1g by overcoming TS7 or into another set of products, that is, c-$CH_2C(NH)C$ + H (channel 1i) in a process without an exit barrier. Finally, by overcoming TS2 associated with ring opening, MIN2 can isomerize to MIN3, located 526 kJ/mol below the reactant energy asymptote. Two different H-loss channels have been identified starting from MIN3, one leading to the CHCCHNH isomer + H (channel 1e, via TS10) and one leading to the linear CH_2CCNH isomer + H (channel 1f, via TS13). MIN3 can also decompose into propargyl radical + NH by fission of its C−N bond (channel 1h). Alternatively, MIN3 can isomerize to MIN4 by overcoming a barrier of +187 kJ/mol (TS3) or to MIN5 by overcoming a barrier of +217 kJ/mol (TS15).

MIN4 can dissociate into HCN + CH_2CH (channel 1b, exothermic by −434 kJ/mol) by overcoming the barrier associated with TS14 or into vinyl cyanide (CH_2CHCN) + H (channel 1a, exothermic by −444 kJ/mol) by overcoming the barrier associated with TS6. MIN4 can also isomerize to MIN5 by overcoming a barrier of 204 kJ/mol (TS4). Once formed, MIN5 can dissociate into HNC + CH_2CH (channel 1d, TS15) through the breaking of a C−C bond or into CH_2CHCN + H (channel 1a, TS11), CH_2CCNH + H (channel 1f), and CHCHCNH + H (channel 1k). Finally, MIN5 can isomerize to MIN6, located 532 kJ/mol below the energy of the

https://doi.org/10.1021/acsearthspacechem.2c00183
ACS Earth Space Chem. XXXX, XXX, XXX−XXX

reactants, overcoming a barrier of 248 kJ/mol (TS9). MIN6 can dissociate by breaking one of the C−H bonds, forming CH_2CCNH + H (channel 1f) or CH_3CCN + H (channel 1h). Alternatively, the breaking of a C−C bond can lead to the formation of CH_3 together with the cofragment CCNH in a barrierless process. Fission of its C−N bond can also lead to CH_3CC + NH in a nearly thermoneutral channel 1n. Finally, one last intermediate has been identified along the PES, MIN7, that can be formed starting from MIN4 after overcoming a barrier of 202 kJ/mol (TS5). MIN7 is the absolute minimum of the PES. The loss of a CN moiety can lead to the formation of ethylene (channel 1c, overall exothermic by 380 kJ/mol). In addition, a barrierless H-loss process can produce the fragment $CHCH_2CN$ (channel 1j) (located 96 kJ/mol below the reactant energy asymptote). Finally, by overcoming of a barrier of 194 kJ/mol (TS12), MIN7 can decompose into atomic hydrogen and vinyl cyanide (channel 1a). All of the identified stationary points lie below the energy level of the reactant asymptote. A schematic representation of the PES is shown in Figure 7, while in Table 2 the reaction enthalpies and barrier heights for each described step are reported, evaluated at the CCSD(T)/aug-cc-pVTZ level of theory considering the geometries optimized at the B3LYP/aug-cc-pVTZ level of theory. The geometries (distances in Angstroms) of the different minima and products identified along the PES together with the main saddle points optimized at the B3LYP/aug-cc-pVTZ level of theory are shown in Figures 8, 9, 10, and 11.

Table 2. Reaction Enthalpies and Barrier Heights (kJ/mol, 0 K) Computed at the CCSD(T)/aug-cc-pVTZ Level of Theory Considering the Geometries Obtained at the B3LYP/aug-cc-pVTZ Level for Dissociation and Isomerization Processes for the System $N(^2D)$ + CH_2CCH_2

	ΔH^0_0 (kJ/mol)	barrier heights (kJ/mol)
$N(^2D)$ + H_2CCCH_2 → MIN1	−507	
MIN1 → MIN2	83	252
MIN2 → MIN3	−102	96
MIN3 → MIN4	−63	188
MIN3 → MIN5	−39	218
MIN4 → MIN5	24	203
MIN4 → MIN7	−33	202
MIN5 → MIN6	34	251
MIN1 → H + c-$CH_2C(N)CH$	281	289
MIN2 → H + c-$CH_2C(NH)C$	328	
MIN2 → H + c-$CH_2C(N)CH$	198	206
MIN3 → H + CHCCHNH	226	236
MIN3 → H + CH_2CCNH	255	258
MIN3 → CH_2CCH + NH	351	
MIN4 → HCN + CH_2CH	155	170
MIN4 → H + CH_2CHCN	145	169
MIN5 → H + CHCHCNH	476	
MIN5 → H + CH_2CCNH	295	
MIN5 → HNC + CH_2CH	198	204
MIN5 → H + CH_2CHCN	122	146
MIN6 → CH_3 + CCNH	461	
MIN6 → H + CH_3CCN	391	
MIN6 → H + CH_2CCNH	261	
MIN6 → CH_3CC + NH	528	
MIN7 → H + $CHCH_2CN$	527	
MIN7 → CN + CH_2CH_2	242	
MIN7 → H + CH_2CHCN	178	194

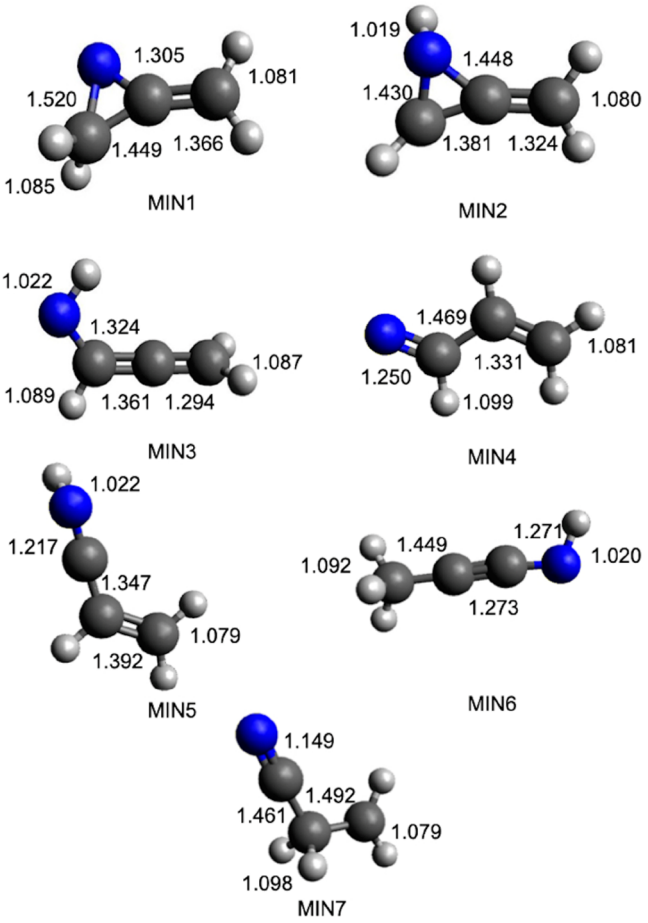

Figure 8. B3LYP-optimized geometries (in Angstroms) of the minima identified along the PES for the reaction $N(^2D)$ + CH_2CCH_2.

We thoroughly searched for a possible H_2-elimination channel originating from one of the PES intermediates. We could not identify any possible route. However, we identified one path for H_2 formation via a roaming mechanism (see Figure 12). The H atom emitted from MIN7 in conjunction with CH_2CHCN formation can wander around and abstract the hydrogen atom of vinyl cyanide in the α position. The transition state, TS_H_2, lies at an energy of −367 kJ/mol with respect to the reactants' asymptote, that is +77 kJ/mol with respect to CH_2CHCN + H.

We tried to verify whether $N(^2D)$ can insert into one of the C−H bonds of allene, but we have been unable to find this pathway. This is in line with previous studies of other systems, where $N(^2D)$ has shown the capability of inserting into C−H sigma bonds when carbon is characterized by sp^3 hybridization (e.g., reactions with methane and ethane), but there are no known cases of insertion into C−H bonds when carbon is sp^2 or sp hybridized (e.g., reactions with ethylene, acetylene, and benzene).

Finally, we characterized the H-abstraction mechanism. At the employed level of calculations, the relative transition state was very close in energy to the reactants. For this reason, we decided to further investigate this reaction at a higher level of accuracy. We optimized the geometry of the transition state and the reactants at the CCSD/cc-pVTZ level; at the same

https://doi.org/10.1021/acsearthspacechem.2c00183
ACS Earth Space Chem. XXXX, XXX, XXX−XXX

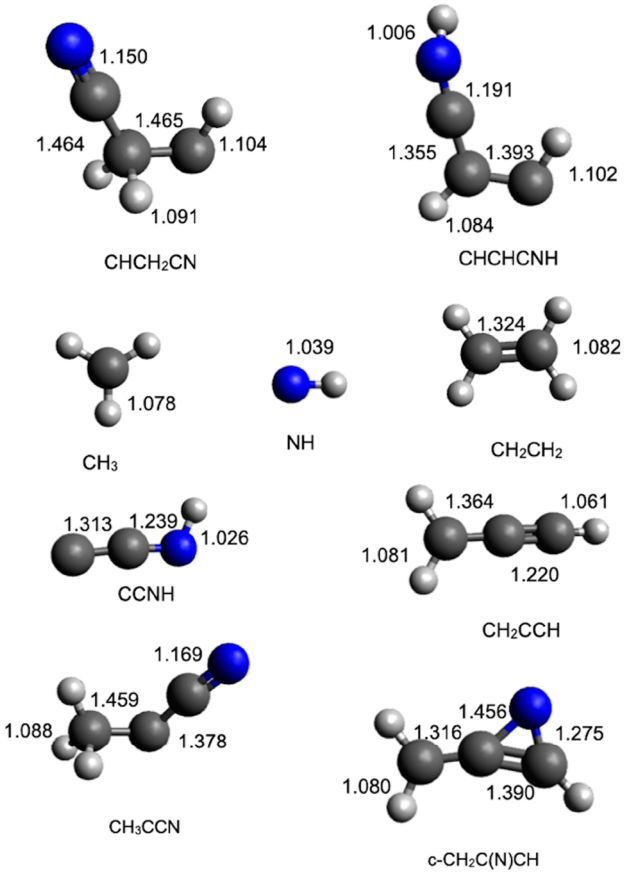

Figure 9. B3LYP-optimized geometries (in Angstroms) of the possible products identified along the PES for the reaction $N(^2D)$ + CH_2CCH_2.

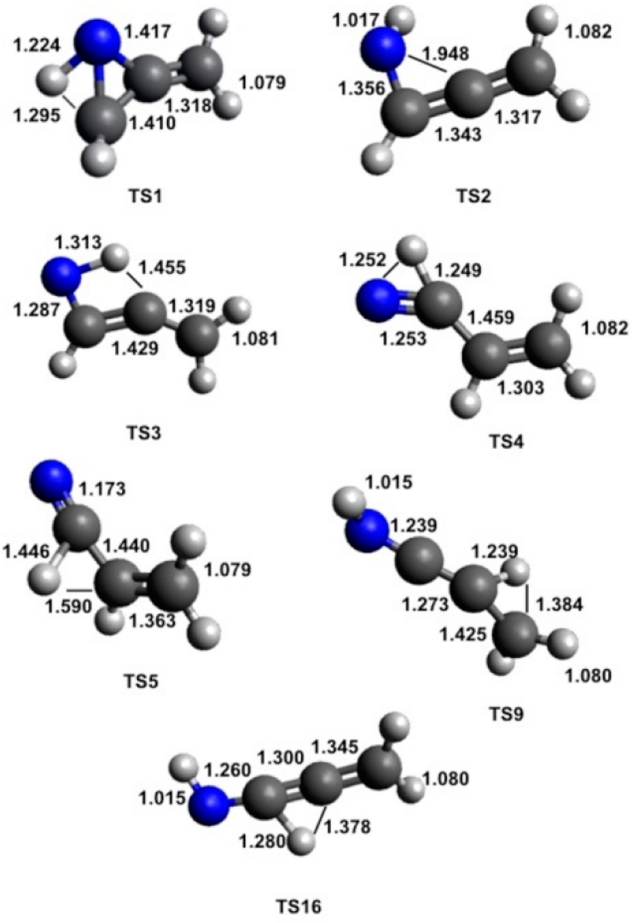

Figure 10. B3LYP-optimized geometries (in Angstroms) of the possible products identified along the PES for the reaction $N(^2D)$ + CH_2CCH_2.

level of accuracy, we computed the vibrational frequencies and the zero-point energy (ZPE) correction. Then, we refined the energetics, evaluating the energy using a modified version[76,77] of Martin's extrapolation scheme[78] in order to extrapolate the energies to the complete basis set (CBS) limit. The energies computed at the CCSD(T)/CBS level were then corrected with ZPE determined at the CCSD/cc-pVTZ level. At this very accurate level of calculation, the transition state for the H-abstraction reaction was computed to be 23.1 kJ/mol above the reactants, suggesting that this reaction cannot be relevant in astrochemical environments where the temperature is very low.

5.2. RRKM Branching Fractions. RRKM estimates of product branching fractions were performed considering the collision energy of the CMB experiment (33 kJ/mol) and for three different temperatures corresponding to the surface temperature of Titan (94 K), its stratospheric temperature (175 K), and room temperature (298 K). As can be seen from electronic structure calculations (Figure 7), the first step of the reaction between $N(^2D)$ and allene is the attack of the nitrogen atom to one of the two equivalent double bonds of allene, leading to formation of the c-$H_2CC(N)CH_2$ intermediate. This intermediate can directly dissociate into the products of channel 1g, or it can undergo several isomerization processes forming both cyclic and linear intermediates. All of the possible elementary processes, including back-isomerization, have been considered in the RRKM calculations to obtain the branching fractions, reported in Table 3. We recall that besides the relative energies of the TS and reactants, the density of states of both TSs and reactants are important factors that influence the values of rate constants (what would roughly correspond to the "entropy of activation").

Under all of the considered conditions, the dominant channel is the one associated with the decomposition into c-$CH_2C(N)CH$ and an H atom (channel 1g) from the first intermediate. The second most important channel is that associated with the fission of a C−H bond from MIN3 leading to the formation of atomic hydrogen and propargyl imine (CHCCHNH) (channel 1e) with a branching fraction value of about 10%. Interestingly, the second dissociation process starting from MIN3 leading to CH_2CCNH + H (channel 1f) does not seem to be competitive. Its branching fraction (also accessible from MIN5 and MIN6) is about 1%. Smaller contributions are associated with the formation routes of HCN and HNC starting from MIN4 and MIN5. The values of the branching fractions for the two pathways (channels 1b and 1d) are about 0.4%, while the formation of vinyl cyanide (channel 1a), which is the most exothermic channel in the potential energy surface, accompanied by the formation of H shows a value of branching fraction of about 0.3%. All of the other contributions can be considered negligible. Is should be noted that given the very small yield of channel 1a, the roaming mechanism that could lead to the formation of H_2 and CH_2CCN is not a significant reaction channel. This is in line

https://doi.org/10.1021/acsearthspacechem.2c00183
ACS Earth Space Chem. XXXX, XXX, XXX−XXX

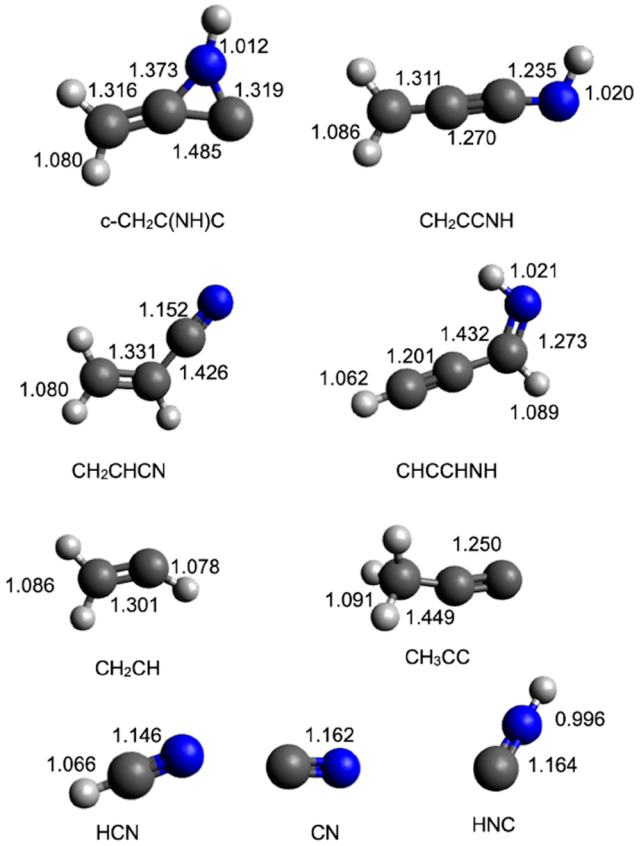

Figure 11. B3LYP-optimized geometries (in Angstroms) of the main transition states identified along the PES for the reaction $N(^2D)$ + CH_2CCH_2.

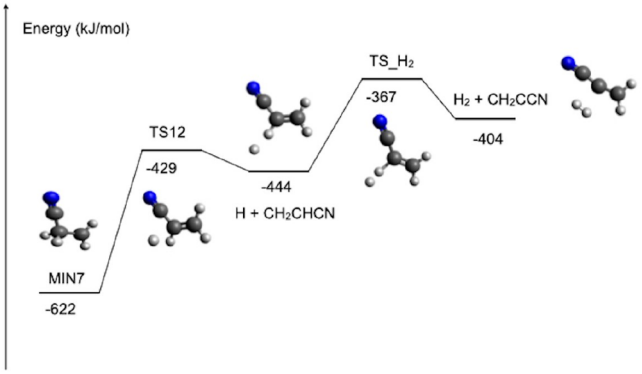

Figure 12. Schematic representation of the roaming mechanism leading to H_2 and CH_2CCN and originating from the interaction of the H atom emitted from MIN7 in conjunction with CH_2CHCN formation (evaluated at the CCSD(T)/aug-cc-pVTZ level of theory, see text).

with the lack of observation of reactive scattering associated with the heavy coproduct at m/z = 52.

Notably, there is little dependence of the products BFs on the energy available to the system.

6. DISCUSSION

As already mentioned, within the sensitivity of our CMB experiments, we did not observe reactive signals associated with HCN, HNC, CN, and CH_3 products, thus indicating that their BFs are smaller than 5−10%. Instead, the experimental data clearly demonstrate that one or more H-displacement channels are occurring. According to our electronic structure calculations, eight isomers with gross formula C_3H_3N can be formed (see sections 3.1 and 5.1). A satisfactory fit of the LAB angular and TOF distributions was achieved by using a single set of CM functions, which implies that our data are not sensitive enough to allow disentangling the possible different contributions originating from more than one channel to the signal at the same mass.

The CM product angular distribution provides us with some information on the reaction mechanism, i.e., its characteristics indicate whether the reaction is direct (that is, it occurs on the time scale of molecular vibrations) or proceeds via the formation of a long-lived complex intermediate[70,79,80] (that is, it occurs within the time necessary for several rotations). Furthermore, the product translational energy distribution is determined by the characteristics of the PES and provide us information on the product energy partitioning between translational and internal degrees of freedom. As already noted in section 4.1, the backward−forward symmetric $T(\theta)$ (Figure 3, top) indicates that the formation of C_3H_3N isomeric products proceeds through a long-lived complex mechanism.[70,79,80] This is fully supported by the reaction PES, which is characterized by bound intermediates associated with deep wells along all possible reaction pathways (see Figure 7). As noted in section 4.1, the shape of the best-fit $T(\theta)$ (and of the functions that still allow an acceptable fit of the experimental data) are in line with the formation of a long-lived complex. Therefore, the expected randomization of the available energy justifies the statistical approach underlying the RRKM method that we used to derive the product branching fractions from the characteristics of the PES.

The energy release, revealed by the shape of the $P(E'_T)$ (Figure 3, bottom), provides us with a criterion (through the energy conservation rule[70]) to establish which channels are responsible for the experimental data. The $P(E'_T)$ cutoff defines the maximum available energy of the products, and the vertical lines represented in Figure 3 (bottom) indicate the total available energy, E_{tot}, for the four most exothermic isomeric channels of interest. Clearly, the best-fit $P(E'_T)$ is consistent with the energetics of four (out of the eight possible) H-displacement channels, namely, channels 1a, 1e, 1f, and 1g. In contrast, the other H-displacement channels 1i−1l can only give a minor contribution. Finally, the cutoff of 335 ± 20 kJ/mol indicates that the most exothermic channel 1a is probably minor with respect to channels 1e, 1f, and 1g.

As can be seen from Table 3, according to RRKM predictions, the three main reaction channels are all H-displacement channels 1e, 1f, 1g with channel 1g, leading to formation of c-$CH_2C(N)CH$, being by far the dominant reaction channel (BF = 87%) under all conditions. The intermediates that can lead to the c-$CH_2C(N)CH$ + H channel are MIN1 and MIN2, but the main pathway is the one associated with MIN1. The competition between dissociation into c-$CH_2C(N)CH$ + H and isomerization to MIN2 is much more in favor of the dissociation despite the fact the barrier associated with product formation (TS8) is 37 kJ/mol higher in energy with respect to the barrier associated with isomerization (TS1). Notably, the most exothermic channel, leading to vinyl cyanide (CH_2CHCN) + H (channel 1a), is theoretically predicted to be negligible (BF = 0.25%) because only a small portion of the reactive flux that reaches MIN3 and

https://doi.org/10.1021/acsearthspacechem.2c00183
ACS Earth Space Chem. XXXX, XXX, XXX−XXX

Table 3. Global Branching Fractions for All Possible Product Channels of the Reaction $N(^2D) + CH_2CCH_2$

reaction channel	products	94 K	175 K	298 K	33 kJ/mol
1a	$CH_2CHCN + H$	0.29%	0.29%	0.28%	0.25%
1b	$C_2H_3 + HCN$	0.43%	0.43%	0.42%	0.38%
1c	$C_2H_4 + CN$	0.01%	0.01%	0.01%	0.01%
1d	$C_2H_3 + HNC$	0.45%	0.45%	0.46%	0.46%
1e	CHCCHNH + H	11.43%	11.36%	11.22%	10.48%
1f	$CH_2CCNH + H$	1.44%	1.44%	1.43%	1.38%
1g	$c\text{-}CH_2C(N)CH + H$	85.95%	86.01%	86.17%	86.96%
1h	CH2CCH + NH	0.00%	0.01%	0.01%	0.08%
1i	$CH_3CCN + H$	0.00%	0.00%	0.00%	0.00%
1j	$c\text{-}CH_2C(NH)C + H$	0.00%	0.00%	0.00%	0.00%
1k	$CHCH_2CN + H$	0.00%	0.00%	0.00%	0.00%
1l	CHCCHNH + H	0.00%	0.00%	0.00%	0.00%
1m	$CH_3 + CCNH$	0.00%	0.00%	0.00%	0.00%
1n	$CH_3CC + NH$	0.00%	0.00%	0.00%	0.00%

MIN3 preferentially dissociates into channel 1e (BF = 10.5%) via TS10 (at −291 kJ/mol respect to reagents) rather than isomerizes to MIN4 (via TS3 at −339 kJ/mol), which is the precursor of channel 1a.

From the product translation energy distribution, we derived the average product translational energy released. If we refer to channel 1g (which has been indicated as the most important one by RRKM estimates of BF), the fraction of product translational excitation, $\langle f'_T \rangle$, is about 0.45 of the total available energy (E_{tot} for each product channel is indicated by a vertical line in Figure 3, bottom). The $\langle f'_T \rangle$ reduces to 0.35 if we refer to the energetics of channel 1e. These values suggest relatively tight exit transition states (TS8, TS13, and TS10 in Figure 1) and the formation of highly internally excited products.

As far as the kinetics of the title reaction is concerned, in common with the reactions of $N(^2D)$ atoms with other unsaturated hydrocarbons such as C_2H_2 and C_2H_4, it can be seen that the rate constants for the $N(^2D)$ + allene reaction are large and independent of temperature, considering the associated experimental uncertainties. Moreover, the carrier gas itself seems to have little or no influence on the measured rates. Consequently, we recommend a temperature-independent value for the rate constant of $1.7 \pm 0.2 \times 10^{-10}$ cm^3 s^{-1} over the 50−300 K range. It should be noted here that the measured rate constant is a sum of reactive and nonreactive "quenching" losses through collisions with CH_2CCH_2. Nevertheless, given the barrierless nature of the reaction and the absence of any substantial submerged barriers over the PES, it is unlikely that quenching plays an important role here.

In Figure 6, we also show the currently recommended values for the rate constants of the $N(^2D)$ + allene reaction as employed in recent photochemical models of Titan's atmosphere by Krasnopolsky[75] and Vuitton et al.[5] These values were estimated by adopting the Arrhenius parameters derived by Sato et al.[24] during their kinetic investigation of the $N(^2D) + C_2H_4$ reaction in a limited range of temperature between 230 and 292 K. We recall that the $N(^2D) + C_2H_4$ reaction has been recently investigated by some of the present authors[22] in the temperature range of interest for Titan, and the values of the rate coefficients were seen to slightly increase with decreasing temperature (the inverse trend in the case of the data by Sato et al.[24]).

Assuming an average temperature of 170 K for the atmosphere of Titan, the rate constant of 1.2×10^{-11} cm^3 s^{-1} (currently recommended in the photochemical models of Titan) is 14 times smaller than the temperature-independent value measured during the present work.

6.1. Comparison with $N(^2D) + CH_3CCH$ (methylacetylene). It is of interest to compare the reaction dynamics of $N(^2D)$ + allene with that of the isomeric reaction $N(^2D)$ + methylacetylene recently studied in our laboratory at a comparable E_c.[18] Methylacetylene and allene are structural isomers that are normally not distinguished in astrochemical or photochemical models, being simply indicated with their gross formula C_3H_4. However, it has been already noted that their formation and destruction routes are indeed different in many cases.[81] In the photochemical model of Titan, methylacetylene and allene are formed through various reactions including

$$H + C_3H_5 \rightarrow CH_3CCH + H_2 \quad (5a)$$

$$\rightarrow CH_2CCH_2 + H_2 \quad (5b)$$

for which a recent estimate of the rate coefficient in the high-pressure limit is 3.4×10^{-10} cm^3 s^{-1}.[82] However, the product branching fraction of reaction 5 has never been derived. In the model by Lavvas et al.,[83] the main formation route of both methylacetylene and allene is as follows

$$CH + C_2H_4 \rightarrow CH_3CCH + H \quad (6a)$$

$$\rightarrow CH_2CCH_2 + H \quad (6b)$$

a fast process where CH_3CCH and CH_2CCH_2 are again assumed to be formed with the same yield. However, experimental studies have shown that the formation of allene was favored in this reaction.[84,85]

Concerning the reactivity of CH_3CCH/CH_2CCH_2, while it is true that their bimolecular reactions are often characterized by similar rate coefficients, the reaction products can be very different. For instance, the dominant product channels of the $O(^3P)$ + methylacetylene and $O(^3P)$ + allene isomeric reactions lead in both cases to CO formation, but the coproducts are singlet ethylidene ($^1CH_3CH$) and singlet ethylene (CH_2CH_2), respectively.[86−88] Another recent example comes from the reaction with the BO radical, where the reaction with methylacetylene features the CH_3-elimination channel as being largely dominant when the exclusive channel for the reaction with allene leads to the formation of CH_2CCHBO in a H-displacement channel.[89]

The case of the reactions with $N(^2D)$ are in the same vein. In the reaction with methylacetylene, the main channels are

https://doi.org/10.1021/acsearthspacechem.2c00183
ACS Earth Space Chem. XXXX, XXX, XXX−XXX

those leading to CH_2NH + C_2H (BF ca. 40%), c-C(N)CH + CH_3 (BF 28−32%), and CH_2CHCN + H (BF 12−16%).[14] Therefore, there are significant differences even though the PESs for the two reactions share some common intermediates. Such a different behavior can be explained by the fact that according to our RRKM calculations, direct decomposition of the first addition intermediate MIN1 is the dominant process in the case of the title reaction, and therefore, the isomerization steps that lead to the formation of the other channels are not competitive. The same is true also for the $N(^2D)$ + methylacetylene reaction[14] that, however, features two possible barrierless attacks leading to two different addition intermediates (one corresponding to bridge addition and one corresponding to the N insertion into one of the C−H bonds of the methyl group). Furthermore, in the case of the $N(^2D)$ + CH_3CCH reaction, there are only three isomerization steps which are necessary to access the most exothermic channel leading to vinyl cyanide and H, all of them favored with respect to their competitive processes, while for the case of the title reaction, four isomerization steps are necessary, starting from the first intermediate, with alternative pathways being more feasible.

7. IMPLICATION FOR THE ATMOSPHERE OF TITAN

To examine the influence of the present measurements on the chemistry of Titan's atmosphere, we included the $N(^2D)$ + allene reaction in a 1D photochemical model described by Dobrijevic et al.,[90] which treats the chemistry of neutrals and cations (we do not consider anions in this study as they play a very minor role), and the coupling between them from the lower atmosphere to the ionosphere. Two different simulations were performed during this investigation. The first one neglected the $N(^2D)$ + allene reaction, which was the case in the previous model. For the second one, we included the $N(^2D)$ + allene reaction using the rate constants ($1.7 \pm 0.2 \times 10^{-10}$ cm^3 s^{-1}) and branching fractions (slightly simplified) determined in this study (see Table 3). As the $N(^2D)$ + allene reaction produces two new species, CHCCHNH and c-$CH_2C(N)CH$, we developed a chemical network to describe these species by considering their most important reactions. For the reactions with barriers, the barrier heights have been calculated theoretically with the Gaussian program[65] using DFT associated with the M06-2X functional and the aug-cc-pVTZ basis set. We also computed the absorption spectra of these species by calculating the energy of the excited states and the oscillator strengths of the transitions from the ground state using the EOM-CCSD(T)/aug-cc-pVTZ method. The main effect of the inclusion of the $N(^2D)$ + allene reaction is the production of the two new species HCCCHNH and c-$CH_2C(N)CH$. Indeed, inclusion of the $N(^2D)$ + allene reaction has only a minor effect on the allene concentration, decreasing its abundance by 8% at 1200 km but very little at low altitude. The integrated column density over the whole atmosphere is only slightly affected (less than 1% decrease). Note that this effect would be even smaller using the rate constant expression recommended by Vuitton et al.[5] The new species produced by the $N(^2D)$ + allene reaction (HCCCHNH and c-$CH_2C(N)CH$) are relatively abundant in the upper atmosphere where $N(^2D)$ is produced. However, their calculated relative abundance are 100 times lower than that of HNC, a species with a similar abundance profile. These low relative abundance limit their possible detection by microwave spectroscopy despite their relatively strong dipole moments calculated around 2.2−2.6 D in both cases. In contrast, the high estimated reactivities of HCCCHNH and c-$CH_2C(N)CH$ with atomic hydrogen and their photodissociation cross sections in the near UV considerably limit their simulated abundance at low altitudes, which would prevent their detection by IR spectroscopy.

We recall that the $N(^2D)$ + allene reaction is considered to produce C_3H_3N (C_2H_3CN in fact) in the modeling study by Vuitton et al.,[5] while the channel leading to C_2H_3CN is negligible according to the present CMB results even if C_2H_3CN is more thermodynamically stable than its isomers HCCCHNH and c-CH_2CNCH.

8. CONCLUSIONS

The $N(^2D)$ reaction with allene was investigated by the CMB technique with mass spectrometric detection at a collision energy of 33 kJ/mol coupled with electronic structure calculations of the underlying potential energy surface. The angular and TOF distributions of C_3H_3N products in the LAB frame along with the derived CM best-fit functions suggest that the reaction mechanism features the formation of one or more C_3H_4N intermediates with lifetimes longer than their rotational periods. The translational energy distribution reveals that C_3H_3N products are internally (ro-vibrationally) excited and that the most exothermic of all possible H-forming channels, namely, cyanoethylene (acrylonitrile or vinylcyanide) + H, is formed with low probability, while other isomers of acrylonitrile are important. Synergistic RRKM statistical calculations on the doublet C_3H_4N PES of product distributions and branching fractions corroborate and complement our findings for the H-displacement channels and provide a more complete picture of the overall reaction mechanism with up to 14 competing product channels being open and for which product BFs are calculated as a function of energy. Of these 14 channels, 9 feature a BF < 1%. Our calculations show that this reaction is initiated by the barrierless addition of the $N(^2D)$ atom to the double bonds of CH_2CCH_2 forming a cyclic adduct complex c-$CH_2C(N)$-CH_2 (MIN1). By the breaking of the C−H bond, this intermediate can directly dissociate predominantly to c-$CH_2C(N)CH$ + H with a predicted BF of about 87% or competitively isomerize to MIN2 and successively to a variety of linear complexes (from MIN3 to MIN7) of which MIN3 dominates, by C−H bond cleavage, to the second and third most important product channels CHCCHNH + H with BF ≈ 10% and CH_2CCNH + H with BF ≈ 1.4%, respectively. All other exothermic channels contribute for well less than 1% (Table 3).

Our studies indicate that the reaction of $N(^2D)$ with CH_2CCH_2, in contrast to the reaction of $N(^2D)$ with the isomer CH_3CCH,[14] is not a potential pathway to produce, in the conditions of the atmosphere of Titan, methanimine (CH_2NH), c-C(N)CH, and acrylonitrile (CH_2CHCN) in the gas phase but rather, via H displacement, predominantly c-$CH_2C(N)CH$, CHCCHNH, and CH_2CCNH.

Kinetic experiments, from room temperature down to 50 K indicated that the rate constants for the $N(^2D)$ + allene reaction are large and independent of temperature, considering the associated experimental uncertainties. We therefore recommend a temperature-independent value for the rate constant of $1.7 \pm 0.2 \times 10^{-10}$ cm^3 s^{-1} over the 50−300 K range. Assuming an average temperature of 170 K for the atmosphere of Titan, this value is 14 times larger than the

https://doi.org/10.1021/acsearthspacechem.2c00183
ACS Earth Space Chem. XXXX, XXX, XXX−XXX

currently recommended[5,6] rate constant of 1.2×10^{-11} cm^3 s^{-1}. While the reaction between $N(^2D)$ and allene has a negligible effect on the simulated abundance of C_2H_3CN, HCCCHNH and c-$CH_2C(N)CH$ are predicted to be relatively abundant in the upper atmosphere where $N(^2D)$ is produced. These species might react further with other molecules acting as precursors for nitriles (C_2N_2, C_3N) or other more complex organic molecules containing a CN bond.

AUTHOR INFORMATION

Corresponding Authors

Nadia Balucani − *Dipartimento di Chimica, Biologia e Biotecnologie, Università degli Studi di Perugia, 06123 Perugia, Italy;* orcid.org/0000-0001-5121-5683; Email: nadia.balucani@unipg.it

Kevin M. Hickson − *Université de Bordeaux, Institut des Sciences Moléculaires, UMR 5255, F-33400 Talence, France; CNRS, Institut des Sciences Moléculaires, UMR 5255, F-33400 Talence, France;* orcid.org/0000-0001-8317-2606; Email: kevin.hickson@u-bordeaux.fr

Authors

Gianmarco Vanuzzo − *Dipartimento di Chimica, Biologia e Biotecnologie, Università degli Studi di Perugia, 06123 Perugia, Italy;* orcid.org/0000-0002-4371-149X

Luca Mancini − *Dipartimento di Chimica, Biologia e Biotecnologie, Università degli Studi di Perugia, 06123 Perugia, Italy*

Giacomo Pannacci − *Dipartimento di Chimica, Biologia e Biotecnologie, Università degli Studi di Perugia, 06123 Perugia, Italy*

Pengxiao Liang − *Dipartimento di Chimica, Biologia e Biotecnologie, Università degli Studi di Perugia, 06123 Perugia, Italy*

Demian Marchione − *Dipartimento di Chimica, Biologia e Biotecnologie, Università degli Studi di Perugia, 06123 Perugia, Italy;* orcid.org/0000-0002-5254-5841

Pedro Recio − *Dipartimento di Chimica, Biologia e Biotecnologie, Università degli Studi di Perugia, 06123 Perugia, Italy;* Present Address: P.R.: Departamento de Química Física, Facultad de Ciencias Químicas, Universidad Complutense de Madrid, 28040 Madrid, Spain; orcid.org/0000-0002-4867-2872

Yuxin Tan − *Dipartimento di Chimica, Biologia e Biotecnologie, Università degli Studi di Perugia, 06123 Perugia, Italy*

Marzio Rosi − *Dipartimento di Ingegneria Civile e Ambientale, Università degli Studi di Perugia, 06100 Perugia, Italy;* orcid.org/0000-0002-1264-3877

Dimitrios Skouteris − *Master-Tec SrL, 06128 Perugia, Italy*

Piergiorgio Casavecchia − *Dipartimento di Chimica, Biologia e Biotecnologie, Università degli Studi di Perugia, 06123 Perugia, Italy;* orcid.org/0000-0003-1934-7891

Jean-Christophe Loison − *Université de Bordeaux, Institut des Sciences Moléculaires, UMR 5255, F-33400 Talence, France; CNRS, Institut des Sciences Moléculaires, UMR 5255, F-33400 Talence, France*

Michel Dobrijevic − *Laboratoire d'Astrophysique de Bordeaux, Université de Bordeaux, CNRS, F-33615 Pessac, France*

Complete contact information is available at: https://pubs.acs.org/10.1021/acsearthspacechem.2c00183

Author Contributions

[§]Y.T.: ERASMUS+ Visiting Ph.D. student from Hefei National Laboratory for Physical Sciences at the Microscale and Department of Chemical Physics, University of Science and Technology of China, Hefei 230026, China.

Author Contributions

The manuscript was written through contributions of all authors. All authors have given approval to the final version of the manuscript.

Notes

The authors declare no competing financial interest.

ACKNOWLEDGMENTS

This work was supported by the Italian Space Agency (ASI, DC-VUM-2017-034, Grant no. 2019-3 U.O. Life in Space). P.L. thanks the European Union's Horizon 2020 Research and Innovation Programme under the Marie Skłodowska-Curie grant agreement no. 811312 for the project "Astro-Chemical Origins" (ACO). K.M.H. acknowledges support from the French program "Physique et Chimie du Milieu Interstellaire" (PCMI) of the CNRS/INSU with the INC/INP cofunded by the CEA and CNES as well as funding from the "Program National de Planétologie" (PNP) of the CNRS/INSU.

REFERENCES

(1) Balucani, N. *Chem. Soc. Rev.* **2012**, *41*, 5473−5483.

(2) Coustenis, A.; Taylor, F. *Titan: The Earth-Like Moon*; World Scientific: Singapore, 1999.

(3) Niemann, H. B.; Atreya, S. K.; Bauer, S. J.; Carignan, G. R.; Demick, J. E.; Frost, R. L.; Gautier, D.; Haberman, J. A.; Harpold, D. N.; Hunten, D. M.; Israel, G.; Lunine, J. I.; Kasprzak, W. T.; Owen, T. C.; Paulkovich, M.; Raulin, F.; Raaen, E.; Way, S. H. The abundances of constituents of Titan's atmosphere from the GCMS instrument on the Huygens probe. *Nature* **2005**, *438*, 779−784.

(4) Loison, J.; Hébrard, E.; Dobrijevic, M.; Hickson, K.; Caralp, F.; Hue, V.; Gronoff, G.; Venot, O.; Bénilan, Y. The neutral photochemistry of nitriles, amines and imines in the atmosphere of Titan. *Icarus* **2015**, *247*, 218−247.

(5) Vuitton, V.; Yelle, R.; Klippenstein, S.; Hörst, S.; Lavvas, P. Simulating the density of organic species in the atmosphere of Titan with a coupled ion-neutral photochemical model. *Icarus Icarus* **2019**, *324*, 120−197.

(6) Dutuit, O.; Carrasco, N.; Thissen, R.; Vuitton, V.; Alcaraz, C.; Pernot, P.; Balucani, N.; Casavecchia, P.; Canosa, A.; Picard, S. L.; et al. Critical review of N, N^+, N^{+2}, N^{+2}, and N^{++2} main production processes and reactions of relevance to Titan's atmosphere. *Astrophys. J. Suppl. Ser.* **2013**, *204*, 20.

(7) Yung, Y. L.; Allen, M.; Pinto, J. P. Photochemistry of the atmosphere of Titan: Comparison between model and observations. *Astrophys. J., Suppl. Ser.* **1984**, *55*, 465−506.

(8) Yung, Y. L. *Icarus* **1987**, *72*, 468−472.

(9) Balucani, N.; Alagia, M.; Cartechini, L.; Casavecchia, P.; Volpi, G. G.; Sato, K.; Takayanagi, T.; Kurosaki, Y. Cyanomethylene formation from the reaction of excited nitrogen atoms with acetylene: a crossed beam and ab initio study. *J. Am. Chem. Soc.* **2000**, *122*, 4443−4450.

(10) Balucani, N.; Cartechini, L.; Alagia, M.; Casavecchia, P.; Volpi, G. G. Observation of Nitrogen-Bearing Organic Molecules from Reactions of Nitrogen Atoms with Hydrocarbons: A Crossed Beam Study of N(2D) + Ethylene. *J. Phys. Chem. A* **2000**, *104*, 5655−5659.

(11) Balucani, N.; Bergeat, A.; Cartechini, L.; Volpi, G. G.; Casavecchia, P.; Skouteris, D.; Rosi, M. Combined crossed molecular beam and theoretical studies of the N (^2D)+ CH_4 reaction and implications for atmospheric models of Titan. *J. Phys. Chem. A* **2009**, *113*, 11138−11152.

(12) Balucani, N.; Leonori, F.; Petrucci, R.; Stazi, M.; Skouteris, D.; Rosi, M.; Casavecchia, P. Formation of nitriles and imines in the atmosphere of Titan: combined crossed-beam and theoretical studies on the reaction dynamics of excited nitrogen atoms N (^{2}D) with ethane. *Faraday Discuss.* **2010**, *147*, 189−216.
(13) Balucani, N.; Skouteris, D.; Leonori, F.; Petrucci, R.; Hamberg, M.; Geppert, W. D.; Casavecchia, P.; Rosi, M. Combined crossed beam and theoretical studies of the N (^{2}D) + C_2H_4 reaction and implications for atmospheric models of Titan. *J. Phys. Chem. A* **2012**, *116*, 10467−10479.
(14) Mancini, L.; Vanuzzo, G.; Marchione, D.; Pannacci, G.; Liang, P.; Recio, P.; Rosi, M.; Skouteris, D.; Casavecchia, P.; Balucani, N. The Reaction N(^{2}D) + CH_3CCH (Methylacetylene): A Combined Crossed Molecular Beams and Theoretical Investigation and Implications for the Atmosphere of Titan. *J. Phys. Chem. A* **2021**, *125*, 8846−8859.
(15) Balucani, N.; Cartechini, L.; Capozza, G.; Segoloni, E.; Casavecchia, P.; Volpi, G. G.; Javier Aoiz, F.; Banares, L.; Honvault, P.; Launay, J.-M. Quantum effects in the differential cross sections for the insertion reaction N(^{2}D) + H_2. *Phys. Rev. Lett.* **2002**, *89*, 013201.
(16) Homayoon, Z.; Bowman, J. M.; Balucani, N.; Casavecchia, P. Quasiclassical trajectory calculations of the N(^{2}D) + H_2O reaction: Elucidating the formation mechanism of HNO and HON seen in molecular beam experiments. *J. Phys. Chem. Lett.* **2014**, *5*, 3508−3513.
(17) Balucani, N.; Cartechini, L.; Casavecchia, P.; Homayoon, Z.; Bowman, J. M. A combined crossed molecular beam and quasiclassical trajectory study of the Titan-relevant N(^{2}D) + D_2O reaction. *Mol. Phys.* **2015**, *113*, 2296−2301.
(18) Liang, P.; Mancini, L.; Marchione, D.; Vanuzzo, G.; Ferlin, F.; Recio, P.; Tan, Y.; Pannacci, G.; Vaccaro, L.; Rosi, M.; et al. Combined crossed molecular beams and computational study on the N(^{2}D) + HCCCN($X^1\sum^+$) reaction and implications for extra-terrestrial environments. *Mol. Phys.* **2022**, *120* (1-2), e1948126.
(19) Recio, P.; Marchione, D.; Caracciolo, A.; Murray, V. J.; Mancini, L.; Rosi, M.; Casavecchia, P.; Balucani, N. A crossed molecular beam investigation of the N(^{2}D) + pyridine reaction and implications for prebiotic chemistry. *Chem. Phys. Lett.* **2021**, *779*, 138852.
(20) Vanuzzo, G.; Marchione, D.; Mancini, L.; Liang, P.; Pannacci, G.; Recio, P.; Tan, Y.; Rosi, M.; Skouteris, D.; Casavecchia, P.; Balucania, N.; et al. The N(^{2}D) + CH_2CHCN (Vinyl Cyanide) Reaction: A Combined Crossed Molecular Beam and Theoretical Study and Implications for the Atmosphere of Titan. *J. Phys. Chem. A* **2022**, *126* (36), 6110−6123.
(21) Nuñez-Reyes, D.; Loison, J.-C.; Hickson, K. M.; Dobrijevic, M. Rate Constants for the N(^{2}D) + C_2H_2 Reaction over the 50−296 K Temperature Range. *Phys. Chem. Chem. Phys.* **2019**, *21*, 22230−22237.
(22) Hickson, K. M.; Bray, C.; Loison, J.-C.; Dobrijevic, M. A Kinetic Study of the N(^{2}D) + C_2H_4 Reaction at Low Temperature. *Phys. Chem. Chem. Phys.* **2020**, *22*, 14026−14035.
(23) Nuñez-Reyes, D.; Loison, J.-C.; Hickson, K. M.; Dobrijevic, M. A Low Temperature Investigation of the N(^{2}D) + CH_4, C_2H_6 and C_3H_8 Reactions. *Phys. Chem. Chem. Phys.* **2019**, *21*, 6574−6581.
(24) Sato, K.; Misawa, K.; Kobayashi, Y.; Matsui, M.; Tsunashima, S.; Kurosaki, Y.; Takayanagi, T. Measurements of Thermal Rate Constants for the Reactions of N(^{2}D,^{2}P) with $C_2H_4$and C_2D_4 between 225 and 292 K. *J. Phys. Chem. A* **1999**, *103*, 8650−8656.
(25) Takayanagi, T.; Kurosaki, Y.; Misawa, K.; Sugiura, M.; Kobayashi, Y.; Sato, K.; Tsunashima, S. Measurements of Thermal Rate Constants and Theoretical Calculations for the N(^{2}D, ^{2}P) + C_2H_2 and C_2D_2 Reactions. *J. Phys. Chem. A* **1998**, *102*, 6251−6258.
(26) Umemoto, H.; Hachiya, N.; Matsunaga, E.; Suda, A.; Kawasaki, M. Rate constants for the deactivation of N(2^{2}D) by simple hydride and deuteride molecules. *Chem. Phys. Lett.* **1998**, *296*, 203−207.
(27) Hanel, R.; Conrath, B.; Flasar, F. M.; Kunde, V.; Maguire, W.; Pearl, J.; Pirraglia, J.; Samuelson, R.; Herath, L.; Allison, M.; Cruikshank, D.; gautier, D.; Gierasch, P.; Horn, L.; Koppany, R.; Ponnamperuma, C. Infrared observations of the Saturnian system from Voyager 1. *Science* **1981**, *212*, 192−200.
(28) Maguire, W.; Hanel, R.; Jennings, D.; Kunde, V. G.; Samuelson, R. E. C_3H_8 and C_3H_4 in Titan's atmosphere. *Nature* **1981**, *292*, 683−686.
(29) Coustenis, A.; Bezard, B.; Gautier, D. Titan's atmosphere from Voyager infrared observations: I. The gas composition of Titan's equatorial region. *Icarus* **1989**, *80*, 54−76.
(30) Nixon, C. A.; Achterberg, R. K.; Teanby, N. A.; Irwin, P. G.; Flaud, J. M.; Kleiner, I.; Dehayem-Kamadjeu, A.; Brown, L. R.; Sams, R. L.; Bézard, B.; Coustenis, A.; Ansty, T. M.; Mamoutkine, A.; Vinatier, S.; Bjoraker, G. L.; Jennings, D. E.; Romani, P. N.; Flasar, F. M. Upper limits for undetected trace species in the stratosphere of Titan. *Faraday Discuss.* **2010**, *147*, 65−81.
(31) Lombardo, N. A.; Nixon, C. A.; Achterberg, R. K.; Jolly, A.; Sung, K.; Irwin, P. G.; Flasar, F. M. Spatial and seasonal variations in C_3H_x hydrocarbon abundance in Titan's stratosphere from Cassini CIRS observations. *Icarus* **2019**, *317*, 454−469.
(32) Roe, H. G.; Greathouse, T.; Tokunaga, A. Update on the TEXES Titan mid-infrared spectral survey. *EPSC-DPS Joint Meeting* **2011**, *6*, EPSC-DPS2011-1398.
(33) Lombardo, N. A.; Nixon, C. A.; Greathouse, T. K.; Bézard, B.; Jolly, A.; Vinatier, S.; Teanby, N. A.; Richter, M. J.; Irwin, P. J. G.; Coustenis, A.; Flasar, F. M. Detection of propadiene on Titan. *Astrophys. J., Lett.* **2019**, *881*, L33.
(34) Casavecchia, P.; Leonori, F.; Balucani, N.; Petrucci, R.; Capozza, G.; Segoloni, E. Probing the Dynamics of Polyatomic Multichannel Elementary Reactions by Crossed Molecular Beam Experiments with Soft Electron-Ionization Mass Spectrometric Detection. *Phys. Chem. Chem. Phys.* **2009**, *11*, 46−65.
(35) Casavecchia, P.; Leonori, F.; Balucani, N. Reaction Dynamics of Oxygen Atoms with Unsaturated Hydrocarbons from Crossed Molecular Beam Studies: Primary Products, Branching Ratios and Role of Intersystem Crossing. *Int. Rev. Phys. Chem.* **2015**, *34*, 161−204.
(36) Leonori, F.; Balucani, N.; Nevrly, V.; Bergeat, A.; Falcinelli, S.; Vanuzzo, G.; Casavecchia, P.; Cavallotti, C. Experimental and Theoretical Studies on the Dynamics of the O (^{3}P)+ Propene Reaction: Primary Products, Branching Ratios, and Role of Intersystem Crossing. *J. Phys. Chem. C* **2015**, *119*, 14632−14652.
(37) Caracciolo, A.; Vanuzzo, G.; Balucani, N.; Stranges, D.; Cavallotti, C.; Casavecchia, P. Observation of H Displacement and H_2 Elimination Channels in the Reaction of O(^{3}P) with 1-Butene from Crossed Beams and Theoretical Studies. *Chem. Phys. Lett.* **2017**, *683*, 105−111.
(38) Sibener, S. J.; Buss, R. J.; Ng, C. Y.; Lee, Y. T. Development of a Supersonic O(^3P_J), O($^1D_2$) Atomic Oxygen Nozzle Beam Source. *Rev. Sci. Instrum.* **1980**, *51*, 167−182.
(39) Alagia, M.; Aquilanti, V.; Ascenzi, D.; Balucani, N.; Cappelletti, D.; Cartechini, L.; Casavecchia, P.; Pirani, F.; Sanchini, G.; Volpi, G. G. Elementary Reactions by Crossed Molecular Beam Experiments with Magnetic Analysis of Supersonic Beams of Atomic Oxygen, Nitrogen, and Chlorine Generated from a Radio-Frequency Discharge. *Israel J. Chem.* **1997**, *37*, 329−342.
(40) Daugey, N.; Caubet, P.; Retail, B.; Costes, M.; Bergeat, A.; Dorthe, G. Kinetic Measurements on Methylidyne Radical Reactions with Several Hydrocarbons at Low Temperatures. *Phys. Chem. Chem. Phys.* **2005**, *7*, 2921−2927.
(41) Daugey, N.; Caubet, P.; Bergeat, A.; Costes, M.; Hickson, K. M. Reaction Kinetics to Low Temperatures. Dicarbon + Acetylene, Methylacetylene, Allene and Propene from 77 ≤ T ≤ 296 K. *Phys. Chem. Chem. Phys.* **2008**, *10*, 729−737.
(42) Shannon, R. J.; Cossou, C.; Loison, J.-C.; Caubet, P.; Balucani, N.; Seakins, P. W.; Wakelam, V.; Hickson, K. M. The Fast C(^{3}P) + CH_3OH Reaction as an Efficient Loss Process for Gas-Phase Interstellar Methanol. *RSC Adv.* **2014**, *4*, 26342.
(43) Hickson, K. M.; Loison, J.-C.; Nuñez-Reyes, D.; Méreau, R. Quantum Tunneling Enhancement of the C + H_2O and C + D_2O

https://doi.org/10.1021/acsearthspacechem.2c00183
ACS Earth Space Chem. XXXX, XXX, XXX−XXX

Reactions at Low Temperature. *J. Phys. Chem. Lett.* **2016**, *7*, 3641−3646.
(44) Bourgalais, J.; Capron, M.; Kailasanathan, R. K. A.; Osborn, D. L.; Hickson, K. M.; Loison, J.-C.; Wakelam, V.; Goulay, F.; Le Picard, S. D. The $C(^3P)$ + NH_3 Reaction in Interstellar Chemistry. I. Investigation of the Product Formation Channels. *Astrophys. J.* **2015**, *812*, 106.
(45) Hickson, K. M.; Loison, J.-C.; Wakelam, V. Temperature Dependent Product Yields for the Spin Forbidden Singlet Channel of the $C(^3P)$ + C_2H_2 Reaction. *Chem. Phys. Lett.* **2016**, *659*, 70−75.
(46) Grondin, R.; Loison, J.-C.; Hickson, K. M. Low Temperature Rate Constants for the Reactions of $O(^1D)$ with N_2, O_2, and Ar. *J. Phys. Chem. A* **2016**, *120*, 4838−4844.
(47) Meng, Q. Y.; Hickson, K. M.; Shao, K. J.; Loison, J. C.; Zhang, D. H. Theoretical and Experimental Investigations of Rate Coefficients of $O(^1D)$ + CH_4 at Low Temperature. *Phys. Chem. Chem. Phys.* **2016**, *18*, 29286−29292.
(48) Nuñez-Reyes, D.; Hickson, K. M. A Low Temperature Investigation of the Gas-Phase N(2D) + NO Reaction. Towards a Viable Source of $N(^2D)$ Atoms for Kinetic Studies in Astrochemistry. *Phys. Chem. Chem. Phys.* **2018**, *20*, 17442−17447.
(49) Lin, C. L.; Kaufman, F. Reactions of Metastable Nitrogen Atoms. *J. Chem. Phys.* **1971**, *55*, 3760−3770.
(50) Suzuki, T.; Shihira, Y.; Sato, T.; Umemoto, H.; Tsunashima, S. Reactions of $N(^2D)$ with H_2 and D_2. *J. Chem. Soc., Faraday Trans* **1993**, *89*, 995−999.
(51) Bergeat, A.; Calvo, T.; Dorthe, G.; Loison, J.-C. Fast-Flow Study of the C + NO and C + O_2 Reactions. *Chem. Phys. Lett.* **1999**, *308*, 7−12.
(52) Nuñez-Reyes, D.; Hickson, K. M. The Reactivity of $C(^1D)$ with Oxygen Bearing Molecules NO and O_2 at Low Temperature. *Chem. Phys. Lett.* **2017**, *687*, 330−335.
(53) Hickson, K. M.; Loison, J.-C.; Lique, F.; Kłos, J. An Experimental and Theoretical Investigation of the $C(^1D)$ + N_2 → $C(^3P)$ + N_2 Quenching Reaction at Low Temperature. *J. Phys. Chem. A* **2016**, *120*, 2504−2513.
(54) Becke, A. D. A new mixing of Hartree−Fock and local density-functional theories. *J. Chem. Phys.* **1993**, *98*, 1372−1377.
(55) Stephens, P. J.; Devlin, F. J.; Chabalowski, C. F.; Frisch, M. J. Ab Initio Calculation of Vibrational Absorption and Circular Dichroism Spectra Using Density Functional Force Fields. *J. Phys. Chem.* **1994**, *98*, 11623−11627.
(56) Dunning, T. H., Jr. Gaussian basis sets for use in correlated molecular calculations. I. The atoms boron through neon and hydrogen. *J. Chem. Phys.* **1989**, *90*, 1007−1023.
(57) Woon, D. E.; Dunning, T. H., Jr. Gaussian basis sets for use in correlated molecular calculations. III. The atoms aluminum through argon. *J. Chem. Phys.* **1993**, *98*, 1358−1371.
(58) Kendall, R. A.; Dunning, T. H., Jr.; Harrison, J. R. Electron affinities of the first-row atoms revisited. Systematic basis sets and wave functions. *J. Chem. Phys.* **1992**, *96*, 6796−6806.
(59) Gonzalez, C.; Schlegel, H. B. An improved algorithm for reaction path following. *J. Chem. Phys.* **1989**, *90*, 2154−2161.
(60) Gonzalez, C.; Schlegel, H. B. Reaction path following in mass-weighted internal coordinates. *J. Phys. Chem.* **1990**, *94*, 5523−5527.
(61) Bartlett, R. J. Many-Body Perturbation Theory and Coupled Cluster Theory for Electron Correlation in Molecules. *Annu. Rev. Phys. Chem.* **1981**, *32*, 359−401.
(62) Raghavachari, K.; Trucks, G. W.; Pople, J. A.; Head-Gordon, M. Quadratic configuration interaction. A general technique for determining electron correlation energies. *Chem. Phys. Lett.* **1989**, *157*, 479−483.
(63) Olsen, J.; Jorgensen, P.; Koch, H.; Balkova, A.; Bartlett, R. J. Full configuration−interaction and state of the art correlation calculations on water in a valence double-zeta basis with polarization functions. *J. Chem. Phys.* **1996**, *104*, 8007−8015.
(64) Schofield, K. Critically evaluated rate constants for gaseous reactions of several electronically excited species. *J. Phys. Chem. Ref. Data* **1979**, *8*, 723−798.
(65) Frisch, M. J.; Trucks, G. W.; Schlegel, H. B.; Scuseria, G. E.; Robb, M. A.; Cheeseman, J. R.; Scalmani, G.; Barone, V.; Mennucci, B.; Petersson, G. A.; et al. *Gaussian 09*, Revision A.02; Gaussian, Inc.: Wallingford CT, 2009.
(66) *Avogadro: an open-source molecular builder and visualization tool*, Version 1.2.0; http://avogadro.cc/.
(67) Hanwell, M. D.; Curtis, D. E.; Lonie, D. C.; Vandermeersch, T.; Zurek, E.; Hutchison, G. R. Avogadro: An advanced semantic chemical editor, visualization, and analysis platform. *J. Cheminf.* **2012**, *4*, 17.
(68) Gilbert, R. G.; Smith, S. C. *Theory of Unimolecular and Recombination Reactions*; Blackwell Scientific Publications, UK, 1990.
(69) Klippenstein, S. J. Variational optimizations in the Rice-Ramsberger-Kassel-Marcus theory calculations for unimolecular dissociations with no reverse barrier. *J. Chem. Phys.* **1992**, *96*, 367.
(70) Levine, R. D.; Bernstein, R. B. *Molecular Reaction Dynamics and Chemical Reactivity*; Oxford University Press: New York, 1987.
(71) Chastaing, D.; Le Picard, S. D.; Sims, I. R.; Smith, I. W. M. Rate Coefficients for the Reactions of $C(^3P_j)$ Atoms with C_2H_2, C_2H_4, $CH_3C{\equiv}CH$ and $H_2C{=}C{=}CH_2$ at Temperatures Down to 15 K. *Astron. Astrophys.* **2001**, *365*, 241−247.
(72) Naulin, C.; Daugey, N.; Hickson, K. M.; Costes, M. Dynamics of the Reactions of $C(^3P_j)$ Atoms with Ethylene, Allene, and Methylacetylene at Low Energy Revealed by Doppler−Fizeau Spectroscopy. *J. Phys. Chem. A* **2009**, *113*, 14447−14457.
(73) Loison, J.-C.; Bergeat, A. Reaction of Carbon Atoms, C ($2p^2$, ^3P) with C_3H_4 (Allene and Methylacetylene), C_3H_6(Propylene) and C_4H_8(Trans-Butene): Overall Rate Constants and Atomic Hydrogen Branching Ratios. *Phys. Chem. Chem. Phys.* **2004**, *6*, 5396−5401.
(74) Balucani, N.; Asvany, O.; Kaiser, R. I.; Osamura, Y. Formation of Three C_4H_3N Isomers from the Reaction of $CN(X^2\Sigma^+)$with Allene, H_2CCCH_2 (X^1A_1), and Methylacetylene, CH_3CCH (X^1A_1): A Combined Crossed Beam and Ab Initio Study. *J. Phys. Chem. A* **2002**, *106*, 4301−4311.
(75) Krasnopolsky, V. A. The Photochemical Model of Titan's Atmosphere and Ionosphere: A Version without Hydrodynamic Escape. *Planetary and Space Science* **2010**, *58*, 1507−1515.
(76) Caracciolo, A.; Vanuzzo, G.; Balucani, N.; Stranges, D.; Tanteri, S.; Cavallotti, C.; Casavecchia, P. Crossed molecular beams and theoretical studies of the O (^3P)+ 1, 2-butadiene reaction: Dominant formation of propene+ CO and ethylidene+ ketene molecular channels. *Chin. J. Chem. Phys.* **2019**, *32*, 113.
(77) Cavallotti, C.; De Falco, C.; Pratali Maffei, L.; Caracciolo, A.; Vanuzzo, G.; Balucani, N.; Casavecchia, P. Theoretical Study of the Extent of Intersystem Crossing in the O (^3P)+ C_6H_6 Reaction with Experimental Validation. *J. Phys. Chem. Lett.* **2020**, *11*, 9621−9628.
(78) Martin, J. M. L. Ab Initio Total Atomization Energies of Small Molecules − Towards the Basis Set Limit. *Chem. Phys. Lett.* **1996**, *259*, 669−678.
(79) Miller, W. B.; Safron, S. A.; Herschbach, D. R. Exchange reactions of alkali atoms with alkali halides: a collision complex mechanism. *Discuss. Faraday Soc.* **1967**, *44*, 108−122.
(80) Fisk, G. A.; McDonald, J. D.; Herschbach, D. R. General discussion. *Discuss.Faraday Soc.* **1967**, *44*, 228−229.
(81) Occhiogrosso, A.; Viti, S.; Balucani, N. An improved chemical scheme for the reactions of atomic oxygen and simple unsaturated hydrocarbons - implications for star-forming regions. *Mon. Not. R. Astron. Soc.* **2013**, *432*, 3423−3430.
(82) Harding, L. B.; Klippenstein, S. J.; Georgievskii, Y. On the Combination Reactions of Hydrogen Atoms with Resonance-Stabilized Hydrocarbon Radicals. *J. Phys. Chem. A* **2007**, *111*, 3789−3801.
(83) Lavvas, P. P.; Coustenis, A.; Vardavas, I. M. Coupling photochemistry with haze formation in Titan's atmosphere, Part II: Results and validation with Cassini/Huygens data. *Planet. Space Sci.* **2008**, *56*, 67−99.
(84) Zhang, F.; Maksyutenko, P.; Kaiser, R. I. Chemical dynamics of the $CH(X^2P)$ + $C_2H_4(X^1A_{1g})$, $CH(X^2P)$ + $C_2D_4(X^1A_{1g})$, and

https://doi.org/10.1021/acsearthspacechem.2c00183
ACS Earth Space Chem. XXXX, XXX, XXX−XXX

$CD(X^2P)$ + $C2H4(X^1A_{1g})$ reactions studied under single collision conditions. *Phys. Chem. Chem. Phys.* **2012**, *14*, 529−537.
(85) Goulay, F.; Trevitt, A. J.; Meloni, G.; Selby, T. M.; Osborn, D. L.; Taatjes, C. A.; Vereecken, L.; Leone, S. R. Cyclic Versus Linear Isomers Produced by Reaction of the Methylidyne Radical (CH) with Small Unsaturated Hydrocarbons. *J. Am. Chem. Soc.* **2009**, *131*, 993−1005.
(86) Vanuzzo, G.; Balucani, N.; Leonori, F.; Stranges, D.; Falcinelli, S.; Bergeat, A.; Casavecchia, P.; Gimondi, I.; Cavallotti, C. Isomer-Specific Chemistry in the Propyne and Allene Reactions with Oxygen Atoms: CH_3CH + CO versus CH_2CH_2 + CO Products. *J. Phys. Chem. Lett.* **2016**, *7*, 1010−1015.
(87) Vanuzzo, G.; Balucani, N.; Leonori, F.; Stranges, D.; Nevrly, V.; Falcinelli, S.; Bergeat, A.; Casavecchia, P.; Cavallotti, C. Reaction Dynamics of $O(^3P)$ + Propyne: I. Primary Products, Branching Ratios, and Role of Intersystem Crossing from Crossed Molecular Beam Experiments. *J. Phys. Chem. A* **2016**, *120*, 4603−4618.
(88) Leonori, F.; Occhiogrosso, A.; Balucani, N.; Bucci, A.; Petrucci, R.; Casavecchia, P. Crossed Molecular Beam Dynamics Studies of the $O(^3P)$ + Allene Reaction: Primary Products, Branching Ratios, and Dominant Role of Intersystem Crossing. *J. Phys. Chem. Lett.* **2012**, *3*, 75−80.
(89) Kaiser, R. I.; Balucani, N. Exploring the Gas Phase Synthesis of the Elusive Class of Boronyls and the Mechanism of Boronyl Radical Reactions under Single Collision Conditions. *Acc. Chem. Res.* **2017**, *50*, 1154−1162.
(90) Dobrijevic, M.; Loison, J. C.; Hickson, K. M.; Gronoff, G. 1D-coupled photochemical model of neutrals, cations and anions in the atmosphere of Titan. *Icarus* **2016**, *268*, 313−339.

https://doi.org/10.1021/acsearthspacechem.2c00183
ACS Earth Space Chem. XXXX, XXX, XXX−XXX